THE UNIVERSITY OF MICHIGAN

INDUSTRY PROGRAM OF THE COLLEGE OF ENGINEERING

THE LEVEL STRUCTURE OF EUROPIUM-153 AND EUROPIUM-155

Raymond E. Sund

A dissertation submitted in partial fulfillment
of the requirements for the degree of
Doctor of Philosophy in The
University of Michigan
1960

September, 1960

IP-463

Doctoral Committee:

Professor Marcellus L. Wiedenbeck, Chairman
Professor H. Richard Crane
Professor Wayne E. Hazen
Assistant Professor Karl T. Hecht
Associate Professor Jack E. McLaughlin

ACKNOWLEDGMENTS

The author wishes to express his sincere appreciation to the following:

Professor M. L. Wiedenbeck for his kind helpfulness and guidance throughout the course of this work;

Dr. Robert G. Arns for his assistance in taking data and much enlightening advice;

L. I. Yin and Kenneth Wright for their help in taking data;

The Rackham Graduate School and the National Science Foundation for making available to him the University Fellowship in Graduate School and the National Science Foundation Cooperative Graduate Fellowship;

The Industry Program of the College of Engineering for reproducing this thesis.

The author also wishes to express his appreciation to the Michigan Memorial-Phoenix Project and the United States Atomic Energy Commission for partial support of this work.

TABLE OF CONTENTS

TABLE OF CONTENTS CONT'D

LIST OF TABLES

LIST OF FIGURES

LIST OF FIGURES CONT'D

CHAPTER I

INTRODUCTION

Background

One of the primary purposes of low energy nuclear physics is to determine the properties of nuclear energy levels and transitions and to relate these properties to nuclear models. The main properties of concern are the angular momentum (spin), parity, lifetime, quadrupole moment, and magnetic moment of the nuclear levels and the angular momentum and relative branching of the transitions connecting these levels. With the experimental techniques available, much progress has been made in establishing reliable data which can be compared to predictions of nuclear models. Empirical results have lead to refinements in models and proposals of new models. Similarily, the predictions of models sometimes aid the experimenter in studying nuclear properties.

The present investigation is concerned with studying the nuclear energy levels in Eu^{153} and Eu^{155}. The transitions connecting the energy levels have been studied by observation of gamma-ray spectra and by means of internal conversion, coincidence, and directional correlation measurements. Several new, weak gamma transitions were observed for both isotopes, and level structures are proposed. Spin assignments are discussed. The results are interpreted in terms of collective motions and intrinsic excitations in deformed nuclei.

The Nuclear Shell Model

The nuclear shell model has been successful in many of its predictions. It was first suggested by Mayer[1] and by Haxel, Jensen, and Suess.[2] This model was advanced primarily as an explanation of the magic numbers at neutron or proton numbers 2, 8, 20, 28, 50, 82, and 126. Nuclei with these numbers of nucleons of the same kind are exceptionally stable. This is analogous to the atomic case, where atoms of 2, 8, 18, ... electrons are particularily stable.

Much empirical evidence for magic numbers is available.[3] One such support is the percentage abundance of the various isotopes occurring in nature. For instance, tin (Z = 50) has ten stable isotopes, which is more than any other element. Calcium (Z = 20) has five isotopes with a spread of eight mass numbers. The large spread in this region of elements shows unusual stability. The neutron capture cross section is unusually low for nuclei with neutron numbers equal to 50, 82, and 126. The binding energy of the odd nucleon in ${}_{36}Kr_{51}^{87}$, and ${}_{54}Xe_{83}^{137}$ is so small that these nuclei are spontaneous neutron emitters. Data on beta decay systematics and alpha decay energies also support the magic numbers.

In the shell model it is assumed that the potential in which a particular nucleon moves is an average, static potential determined by the rest of the nucleons. Since the nuclear forces are not well known, plausible assumptions are made about the potential. These are: no singularity at the center of gravity ($r = 0$), $\frac{\partial V}{\partial r} = 0$ at $r = 0$, spherical symmetry, and a fast change in the potential at the nuclear boundary.[4] Two simple potentials which fulfill these requirements are the isotropic

harmonic oscillator potential and the square-well potential. The energy levels for these two potentials are much alike, particularily for the low levels. Other potentials which fulfill the above conditions lead to similar results.

The energy level of each nucleon can be characterized by quantum numbers (n, ℓ, j, m_j), where n is the radial quantum number, ℓ is the orbital angular momentum quantum number, j is the total angular momentum quantum number, and m_j is the quantum number for quantization of direction. The energy levels are filled with protons and neutrons independently, according to Pauli's exclusion principle. Each level is $(2j + 1)$ degenerate.

Wide gaps take place in the energy levels after 2, 8, and 20 protons (or neutrons). This agrees with the known data on magic numbers. However, the potential does not explain the magic numbers at 50, 82, and 126. In order to account for this information, a strong spin-orbit coupling was assumed. This coupling splits every ℓ level into two levels with $j = \ell \pm \frac{1}{2}$. The level with $j = \ell + \frac{1}{2}$ has the lower energy, and the energy difference between the $\ell + \frac{1}{2}$ and $\ell - \frac{1}{2}$ states increases with ℓ.[4]

According to the shell model, all closed shells and subshells (with $2j + 1$ nucleons in a particular j orbit) are spherically symmetric, so every filled level has a total angular momentum zero. A nucleus containing an extra nucleon in addition to the filled proton and neutron levels has a total angular momentum equal to that of the extra nucleon.

For nuclei with several nucleons outside closed shells or subshells, additional coupling rules are given. One such rule is that an even number of neutrons or protons having a certain value of j pair off

their angular momenta such that the resulting ground state angular momentum is zero.[5] This agrees with the ground state angular momentum of zero for nuclei with an even number of neutrons and protons. In odd-A nuclei, the nucleons will usually couple their angular momenta such that the total ground state angular momentum is that of the last partially filled orbit.

The previous rules predict the parity of the ground state as well as the spin. The parity of an individual particle state is odd if ℓ is odd and even if ℓ is even. The parity of the nucleus is the product of all the nucleon parity quantum numbers. Therefore, all levels with an even number of particles have even parity.

The agreement between the experimental data and the predictions of the shell model for spin and parity assignments of the ground states is particularily good for isotopes near closed shells.[3]

The spins and parities of low-lying states of nuclei may sometimes be predicted from the low, empty energy levels available.

Predictions for the magnetic moment of a nucleus with an odd nucleon may be made on the basis of the contribution from the orbital motion (for a proton) and from the intrinsic magnetic moment of the odd nucleon. These predictions give qualitative agreement with the experimental measurements.[3] The deviations indicate the approximate nature of the model.

Although the shell model is very successful in many of its predictions, it has several failures besides the deviations previously mentioned. One such case is in regard to the quadrupole moment, which is defined[3] as

$$Q = \frac{1}{e} \int r^2(3 \cos^2\theta - 1)\, \rho(\vec{r})_{M=J}\, d\tau \qquad (1)$$

where $\rho(\vec{r})$ is the charge density, θ is the angle between the z axis and the radius vector to any point in the nucleus, e is the unit of charge for a proton, and $d\tau$ is a volume element. In the shell model the value of Q depends on the last odd nucleon and is approximately proportional to the square of the nuclear radius for the case of an odd proton. Quadrupole moments much larger than this have been observed for heavy nuclei. For an odd-neutron nucleus, only the slow rotation of the core as a reaction to the neutron motion should have an effect. Since the charge to mass ratio of the nuclear core is about one-half that of protons and the rotational speed is about 1/A of the odd neutron, the Q value for an odd-neutron neucleus would be expected to be about 1/2A of that for an odd-proton nucleus.(5) However, the quadrupole moments of odd-neutron and odd-proton nuclei are similar.

Another difficulty with the shell model is in regard to the transition probabilities of electric quadrupole gamma rays occurring in even-even nuclei. The quadrupole moments related to such transitions are typically much larger than the possible moments for single-proton transitions.

The energies of the first excited state in even-even nuclei are large in the region of closed-shell nuclei. The energies are particularily low for a mass number between 150 and 190 and greater than 222. The shell structure fails to explain this.

The Collective Nuclear Model

Some of the failures in the shell model predictions may be explained by a model based on the collective motion of nucleons. In the shell model the field is considered static, and the nucleons interact only to a small extent with each other. In the collective model the nucleus is considered to be made of a core of nucleons in closed shells and of the extra nucleons which move in the core potential. Due to the interaction of the extra nucleons with the core, the core is deformed. In turn, the field of the deformed core affects the motion of the extra nucleons. Rotational and intrinsic excitations have been postulated. The rotational motion preserves the internal structure of the nucleus. The intrinsic excitations are associated with the individual particle excitations or with collective vibrations about the nuclear equilibrium shape.

The theory for the rotational spectrum of axially symmetric nuclei has been well developed.[6-9] The rotational motion is characterized by the quantum numbers I, K, and M, representing the total angular momentum, its projection on the nuclear symmetry axis, and its projection on the space fixed axis respectively. The quantum number K is a constant for each rotational band. The rotational spectrum is

$$E_I = E_o + \frac{\hbar^2}{2\iota}\left\{I(I+1) + a(-1)^{I+1/2}(I+1/2)\delta_{K,1/2}\right\}, \quad (2)$$

where E_o is a constant which depends on the intrinsic structure, and ι is the effective moment of inertia about an axis perpendicular to the nuclear symmetry axis.[9] The value of ι increases with the number of nucleons outside closed shells. The parameter a is a decoupling parameter for states with $K = 1/2$.

Due to the reflection symmetry of an axially symmetric nucleus, the rotational motion has even parity. Therefore, the parity is determined by that of the particle structure. For an even-even nucleus, the ground state has K = 0, and the lowest rotational band is given by Equation (2), with I = 0, 2, 4, 6, ... , and even parity.(7)

For odd-odd nuclei and odd-even nuclei the spectrum is also given by Equation (2), with $I = I_o$, $I_o + 1$, $I_o + 2$, ... , and with the parity the same as the ground state. In this case K equals the ground state spin I_o. A similar result also holds for the rotational spectrum corresponding to excited particle states in even-even nuclei.

Such rotational spectra are found to occur(9) for $A \sim 25$, $150 < A < 190$, and $A > 222$. Here the nuclei in general have large deformations due to many nucleons outside closed shells. For nuclei with smaller deformations and larger rotational frequencies, the intrinsic nuclear structure is excited by the rotational motion, and the rotational spectrum is no longer strictly applicable.

Strongly deformed nuclei are expected to exhibit distinct types of excitation corresponding to individual particle excitations, collective vibrations, and collective rotations. The energies associated with individual particle excitations are on the order of several hundred kev, which is comparable to energies associated with rotational excitations. Collective vibrational energies occur with an energy on the order of 1 or 2 Mev.(8)

The usual selection rules on spins and parities of transitions exist. In addition, the change in the K value between the initial and final

states should be equal or less than the multipolarity of the transition. This selection rule tends to hinder, rather than completely forbid a transition.

The large electric quadrupole moments observed in the region of deformed nuclei may be explained by the comparatively large number of nucleons outside the core. The collective model has also been successful in predicting transition probabilities between rotational levels.[8,9]

The vibrations are characterized by λ and ν, which correspond to the multipole order and the component of the angular momentum around the symmetry axis respectively.[9] In the case of quadrupole vibrations in even-even nuclei, a band with spins of 0+, 2+, 4+, 6+, ... , and another band with spins of 2+, 3+, 4+, ... are predicted.

Vibrational levels have also been proposed in the region of closed shells.[9,10] For an even-even nucleus, the first excited state is expected to have a spin of 2+, and the second excited state is expected to be a degenerate triplet with spins of 0, 2, 4+. The degeneracies and equally spaced energy levels in such a spectrum are a result of using a harmonic oscillator approximation in the computations. The excitations have electric transition probabilities which are much larger than the single particle estimates.

Recently, Davydov and Filippov[11,12] have investigated the theory of even-even nuclei which are not axially symmetric. They have treated the nucleus as an asymmetric top and have studied the resulting rotational level structure. The assumption was made that the internal state of the nucleus does not change under rotation. Since there is no

symmetry axis, K is no longer a good quantum number. The shape parameter, ν, indicates the deviation of the nuclear shape from axial symmetry. The value of zero for ν corresponds to axial symmetry. A plot of the rotational energy levels versus ν shows the same energy levels as are predicted for an axially symmetric nucleus. The 2+, 4+, and 6+ states increase slightly in energy as ν changes from 0° to 30°. In addition, energy levels with spins 2, 3, 4, ... lie very high for low values of ν. As ν increases, these levels decrease rapidly. Thus, the energy ratio of the second excited state with spin 2 compared to the first state with spin 2 varies from infinity to two as ν increases from 0° to 30°.

The lowest two levels with spins equal to 2 which occur in nuclei between the closed shell and rotational regions have previously been attributed to vibrations of the nuclear surface. Davydov and Filippov have computed the ratio of the reduced electric quadrupole transition probabilities from the second spin 2 state to the ground state and to the first spin 2 state. A comparison of the theoretical predictions with experimental data shows remarkable agreement with nuclei in the intermediate and rotational regions.(13)

Good agreement also exists for the predicted energy of the lowest spin 3 state.(13)

CHAPTER II

INTRINSIC EXCITED STATES IN DEFORMED NUCLEI

In the shell model the nuclear potential is considered to be isotropic. However, it has been pointed out that nuclei with many protons or neutrons outside closed shells have deformed shapes. As a consequence, the deformed nuclear potential is expected to influence the motion of the individual nucleons. Nilsson[14] has considered the nuclear energy levels for nucleons due to such deformed nuclear potentials. A spheroidal harmonic oscillator potential with suitable coupling terms is assumed. The Hamiltonian is then written as the sum of a spherically symmetric term and terms containing the deformation and coupling effects. The eigenvectors of a three-dimensional isotropic harmonic oscillator are used as a basic set in calculating the single-particle eigenvalues and eigenfunctions. The following arguments are due to Nilsson.[14]

The single particle Hamiltonian for a nucleon interacting with the nuclear field is assumed to be of the following type:

$$H = H_o + C\vec{\ell}\cdot\vec{s} + D\vec{\ell}^2 \quad , \tag{1}$$

where

$$H_o = -\frac{\hbar^2}{2M}\Delta' + \frac{M}{2}(\omega_x^2 x'^2 + \omega_y^2 y'^2 + \omega_z^2 z'^2), \tag{2}$$

in which $\vec{s}$ and $\vec{\ell}$ are the spin and orbital angular momentum, respectively, and x', y', and z' are the particle coordinates in a coordinate system fixed in the nucleus. The effect of the $\vec{\ell}^2$ term is that the energy levels lie somewhere between those obtained for an oscillator potential and a square-well potential. For a spherically symmetric harmonic oscillator

potential the level sequence must agree with that of the shell model. This strongly limits the values of C and D.

For the case of cylindrical symmetry

$$\begin{aligned} \omega_x^2 &= \omega_y^2 = \omega_o^2\left(1 + \frac{2}{3}\delta\right) \quad , \\ \omega_z^2 &= \omega_o^2\left(1 - \frac{4}{3}\delta\right) \quad , \end{aligned} \tag{3}$$

where the deformation parameter, δ, is introduced. The assumption of constant volume for the nucleus leads to the condition that $\omega_x\omega_y\omega_z$ is a constant. As a result,

$$\omega_o(\delta) = \overset{o}{\omega}_o\left(1 - \frac{4}{3}\delta^2 - \frac{16}{27}\delta^3\right)^{-1/6} \quad , \tag{4}$$

where

$$\overset{o}{\omega}_o = \omega_o(\delta) \quad \text{for} \quad \delta = 0.$$

New coordinates are introduced, such that

$$x = \sqrt{\frac{M\omega_o}{\hbar}}\, x', \quad \text{etc.} \tag{5}$$

and H_o is split into the sum of a spherically symmetric term $\overset{o}{H}_o$ and a deformation term H_δ, where

$$\begin{aligned} \overset{o}{H}_o &= \frac{\hbar\omega_o}{2}\left(-\Delta + r^2\right) \quad , \\ H_\delta &= -\delta\hbar\omega_o\,\frac{4}{3}\sqrt{\frac{\pi}{5}}\; r^2\, Y_{20} \quad . \end{aligned} \tag{6}$$

The spherical harmonic Y_{20} equals $\frac{1}{4}\sqrt{\frac{5}{\pi}}\,(3\cos^2\theta - 1)$.

The operators commuting with $\overset{o}{H}_o$ are $\vec{\ell}$, ℓ_z, and s_z, with quantum numbers ℓ, Λ, and Σ respectively. The operator $j_z = \ell_z + s_z$, with quantum number $\Omega = \Lambda + \Sigma$, commutes with the total Hamiltonian. The states corresponding to a given Ω are given in terms of the base vectors $|N\ell\Lambda\Sigma>$,

where N is the quantum number for the total number of oscillator quanta.

The following notation is introduced:

$$\kappa = -\frac{1}{2}\frac{C}{\hbar\omega_o^o}, \quad \mu = \frac{2D}{C}, \quad \eta = \frac{\delta}{\kappa}\frac{\omega_o(\delta)}{\omega_o^o}, \quad U = -\frac{4}{3}\sqrt{\frac{\pi}{5}}\, r^2 Y_{20}. \tag{7}$$

Then

$$H - H_o^o = \kappa\hbar\omega_o^o R, \tag{8}$$

where

$$R = \eta U - 2\vec{\ell}\cdot\vec{s} - \mu\vec{\ell}^2. \tag{9}$$

The matrix R is diagonalized in the representation chosen for different values of η, and eigenvalues $r_\alpha^{N\Omega}(\eta)$ are obtained, where α gives the number of the different eigenvalues. Since

$$H_o^o |N\ell\Lambda\Sigma> = (N + \tfrac{3}{2})\hbar\omega_o |N\ell\Lambda\Sigma>, \tag{10}$$

then

$$E_\alpha^{N\Omega} = (N_\alpha + \tfrac{3}{2})\hbar\omega_o(\delta) + \kappa\hbar\omega_o^o r_\alpha^{N\Omega}. \tag{11}$$

The values of κ and μ are chosen so that the level sequence for $\delta = 0$ corresponds to the shell model case. Slightly different parameters are needed to reproduce the neutron and proton spectra. Figures 1 and 2 illustrate the spectra for protons and neutrons, respectively, as a function of nuclear deformation.[15]

States near $\delta = 0$ may be labelled by quantum numbers ℓ and j. For larger values of δ the states of different ℓ and j couple together. For large deformations one may consider the $\vec{\ell}\cdot\vec{s}$ and $\vec{\ell}^2$ terms as perturbations of an anisotropic harmonic oscillator. In this case the quantum numbers

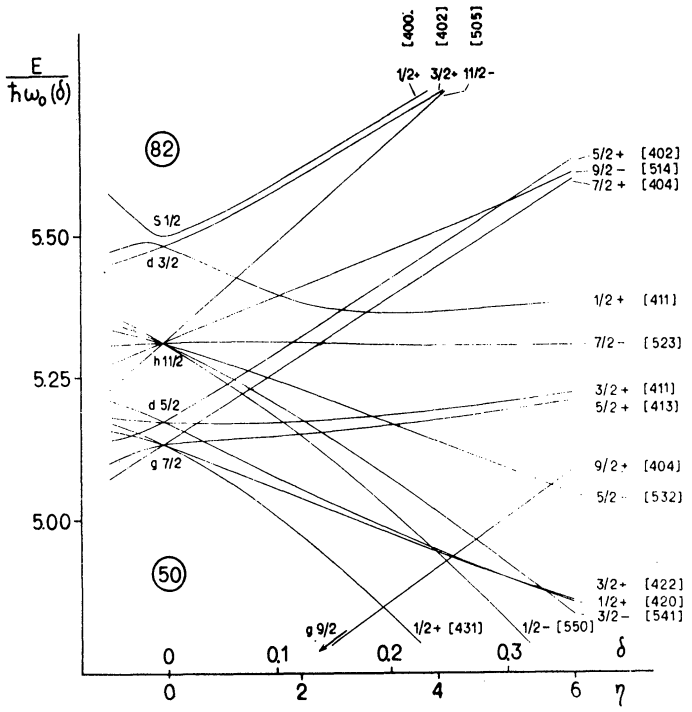

Figure 1. Single-particle levels for odd-Z nuclei in the region $50 < Z < 82$, from M ttelson and Nilsson.[15] The levels are labeled by the parity and by the component of the angular momentum of the nucleon along the nuclear symmetry axis. The numbers in brackets are the asymptotic quantum numbers $[N\ n_z\ \Lambda]$ for deformed nuclei.

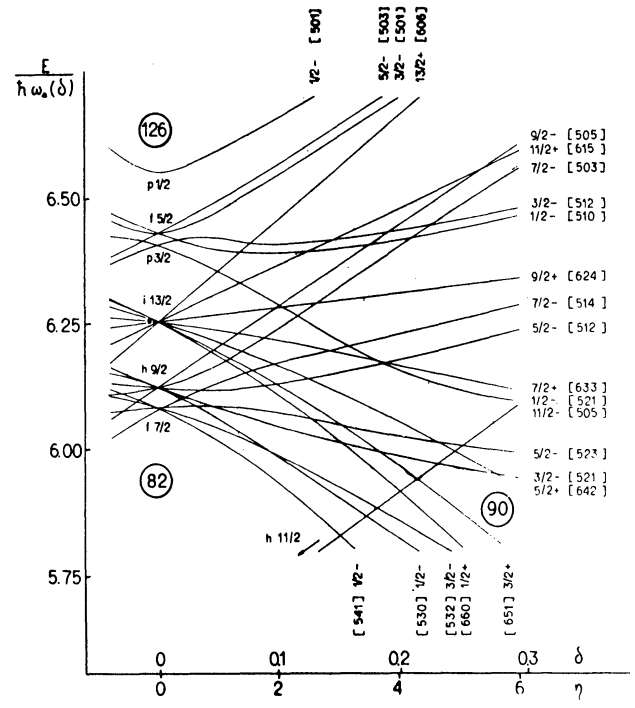

Figure 2. Single-particle levels for odd-N nuclei in the region $82 < N < 126$, from Mottelson and Nilsson.[15] The labeling is the sume as in Figure 1.

N, n_z, Λ and Σ may be used in labeling the states, where n_z is the number of oscillator quanta along the symmetry axis.

The energy levels shown in Figures 1 and 2 are labelled by Ω, the parity, and the asymptotic quantum numbers. Since the only degeneracy is due to the two possible signs of Ω, a simple coupling scheme is implied. In the case of odd-A nuclei, the ground state spin and parity are generally equal to the values for the orbit which the last odd nucleon occupies.(16)

The value of δ for a particular nucleus may be obtained from the measured electric quadrupole moment Q_o and from the relation

$$Q_o = \frac{4}{5} Z R_o^2 \delta(1 + \frac{1}{2}\delta + \ldots), \qquad (12)$$

where R_o is the mean nuclear radius, which is taken to be $1.2\ A^{1/3} 10^{-13}$ cm.(16)

A theoretical estimate of the deformation may be obtained by considering the total energy of the nucleus as a function of deformation. This energy, $\epsilon(\delta)$, may be determined from the spectra of energy levels for nucleons as a function of deformation, taking into account the interaction between nucleons. The equilibrium deformation is given by $(\frac{\partial \epsilon(\delta)}{\partial \delta})_{\delta_{eq.}} = 0$. The deformations obtained in this manner agree well with the values calculated from the nuclear quadrupole moments. The deformations correspond to prolate shapes for the nuclei considered ($A \sim 25$, $150 < A < 190$, and $A > 222$).(16)

Using Figures 1 and 2, the expected ground state spin for an odd-A nucleus may be obtained, provided the deformation is known. If several possible energy levels for the last odd nucleon occur closely spaced, the ground state spin may correspond to either level. In this case a low-lying intrinsic excited state with the spin of the second state is expected to exist.

On each particle level there is superimposed a vibrational band. In addition, a rotational band may be superimposed on each level.

The measured nuclear spins of isotopes in the deformed regions agree well with the Nilsson spin predictions.[15,16]

As already discussed, for sufficiently large deformations the intrinsic states may be approximately classified by the quantum numbers N, n_z, Λ, and Σ. Alaga[17,18] has determined the selection rules associated with these quantum numbers for the case $\Delta I = \Delta\Sigma$. Due to the neglected terms in the Hamiltonian, the selection rules tend to hinder transitions rather than to forbid them. Therefore, the transitions which are permitted by all of the selection rules are called unhindered transitions. Those which are permitted by Ω and I selection rules, but forbidden by any of the other selection rules, are called hindered transitions.

CHAPTER III

GAMMA-GAMMA DIRECTIONAL CORRELATION

Introduction

Angular correlation is a useful experimental technique for studying the properties of nuclear levels and the angular momenta of the radiations. It consists of measuring the coincidence rate between two successive radiations as a function of the angle between the directions of emission.

The probability of emission of a particle or quantum from a radioactive nucleus in general depends on the angle between the direction of emission and the nuclear spin. Ordinarily, a collection of nuclei has randomly oriented spins, so the total emission of quanta is isotropic. In certain situations a strong field may be used to orientate the nuclei. Also, if two quanta are emitted successively in a very short time, the detection of the first quantum in a certain direction selects an ensamble of nuclei with a preferred spin direction. Then the second quantum will in general show a preferred direction of emission or an angular correlation with respect to the first quantum.

Among the various types of angular correlation measurements are gamma-gamma, alpha-gamma, beta-gamma, and conversion electron-gamma correlations. The term gamma-gamma angular correlation usually includes polarization and directional correlations. In polarization correlations the parity of the radiation as well as the angular momentum can be determined. In directional correlation measurements the coincidence rate is determined

only as a function of the angle between two detectors. From such measurements predictions about the spins of the nuclear states as well as the angular momenta of the radiations can be made.

The theory of directional correlation for pure-multipole cascades was first treated by Hamilton[19] in 1940. Early experiments failed due to inadequate experimental techniques. Brady and Deutsch[20] performed the first successful measurement in 1947 by using Geiger tubes. The introduction of scintillation counters in 1948 has greatly stimulated the development of this field.

Elementary Theory of Gamma-Gamma Directional Correlation

The general theory of gamma-gamma directional correlation has been well developed.[19,22-29] The following elementary approach is due to Frauenfelder[29] and gives some insights into the problem.

Consider a gamma transition of angular momentum $\vec{L}$ between two nuclear levels B and C. The projection of $\vec{L}$ on an arbitrary axis (taken as the z axis) is denoted as L_z. The gamma ray is characterized by the orbital momentum quantum number L and the magnetic quantum number M, where $\vec{L}^2 = L(L+1)\hbar^2$ and $\vec{L}_z = M\hbar$. The states B and C have spins $\vec{I}_b$ and $\vec{I}_c$ and are characterized by quantum numbers I_b, m_b and I_c, m_c. The following relationships exist:

$$\begin{aligned} \vec{I}_b &= \vec{L} + \vec{I}_c \\ m_b &= M + m_c \end{aligned} \qquad (1)$$

A certain directional distribution $F_L^M(\theta)$ exists for each $m_b \rightarrow m_c$ transition. Here θ is the angle between the direction of emission and the

z axis. The function F may be determined by calculating the energy flow (Poynting vector) as a function of angle for multipole radiation corresponding to L and M. Since it is impossible to separate the various $m_b \rightarrow m_c$ components in the nuclear case, one always observes the directional distribution $F_L(\theta)$ due to all of the possible transitions between magnetic sublevels. Let $P(m_b)$ be the relative population of each sublevel m_b, and $G(m_b, m_c)$ be the relative transition probability for the $m_b \rightarrow m_c$ transition. Then

$$F_L(\theta) \sim \sum_{m_b m_c} P(m_b) G(m_b, m_c) F_L^M(\theta) \quad , \tag{2}$$

where

$$M = m_b - m_c$$

The factor $G(m_b, m_c)$ depends explicitly on m_b and m_c and not on nuclear properties. Using group theoretical methods, it can be shown that $G(m_b, m_c)$ is equal to the square of the Clebsch-Gordan coefficient for $\vec{I}_b = \vec{I}_c + \vec{L}$ and $m_b = m_c + M$:

$$G(m_b, m_c) = (I_c L m_c M | I_b m_b)^2 \tag{3}$$

The values of $P(m_b)$ depend on the energies of the m_b states and on the manner in which level B is created. For randomly oriented nuclei, all of the m_b levels are equally populated for any z axis, and the distribution $F_L(\theta)$ is isotropic.

Assume that two gamma rays of multipolarity L_1 and L_2 are emitted in a cascade between nuclear levels $A \rightarrow B \rightarrow C$. If the direction of emission of the first gamma ray is taken along the z axis, then the directional correlation $W(\theta)$ between the two gamma rays is equal to $F_{L_2}(\theta)$, the direction distribution of the second gamma ray with respect to the z axis.

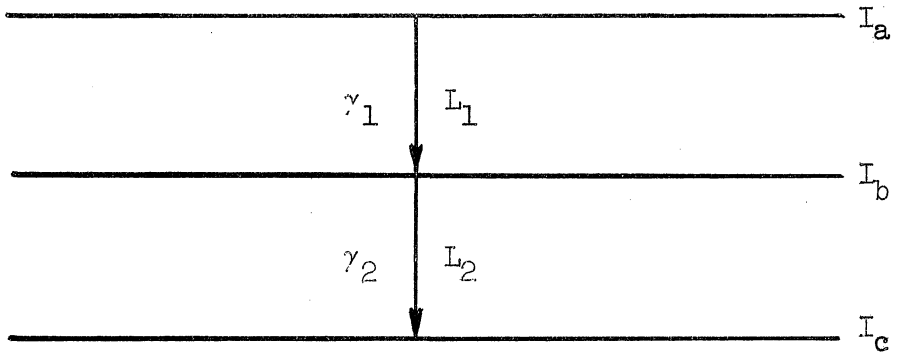

Assuming that the m_a states are equally populated,

$$P(m_b) \sim \sum_{m_a} G(m_a, m_b)\, F_{L_1}^{M_1}(\theta = 0) \quad , \tag{4}$$

where

$$M_1 = m_a - m_b \quad .$$

Since a photon can have angular momentum of only $+\hbar$ or $-\hbar$ in its direction of propagation,[30] the value of M_1 is restricted to ± 1, and only the function $F_{L_1}^{\pm 1}(0)$ occurs in Equation (4).

From Equations (2), (3), and (4),

$$W(\theta) \sim \sum_{m_b m_c m_a} (I_b L_1 m_b \pm 1 \mid I_a m_a)^2\, F_{L_1}^{\pm 1}(0)(I_c L_2 m_c M_2 \mid I_b m_b)^2\, F_{L_2}^{M_2}(\theta) \quad , \tag{5}$$

with

$$M_2 = m_b - m_c \quad .$$

From the above formulae it can be seen that $W(\theta)$ depends on the spins of the three levels and the angular momenta of the radiations. An angular correlation cannot make definite predictions about these five parameters unless additional experimental information is available.

Since $F_L^M(\theta)$ can be expressed in powers of $\cos^2\theta$, $W(\theta)$ is a function of powers of $\cos^2\theta$. It is convenient to express $W(\theta)$ in terms of a series of even order Legendre polynomials.

In the previous discussion it was assumed that the nuclei are not disturbed by extranuclear fields. Then the m_b states of the intermediate level are not repopulated between the emission of the two gamma rays. Otherwise, the information obtained by the first detector in regard to the relative population of the magnetic sublevels will be partially lost, and the correlation will be attenuated. If the lifetime of the intermediate state is less than about 10^{-11} sec., no attenuation will exist. For states with longer lifetimes, a suitable environment, such as a solution or a cubic crystal, must be used in order to obtain an unperturbed correlation.

The function $W(\theta)$ does not depend on the parities of the nuclear states, since electric and magnetic radiations of the same L are related by the transformation $\vec{E} \rightarrow \vec{H}$ and $\vec{H} \rightarrow -\vec{E}$. This transformation does not affect the Poynting vector, so the angular distribution of radiation is not changed. Thus, electric and magnetic radiation cannot be distinguished in a directional correlation measurement.

Hamilton[19] evaluated $W(\theta)$ for all cascades envolving pure dipole and quadruple gamma rays. However, tedious summations over the magnetic quantum numbers are envolved for transitions higher than quadrupole. This difficulty was overcome in the further development and generalization of the theory. In addition, angular correlation theory was extended to include radiations other than gamma rays.

Theoretical Results for Gamma-Gamma Directional Correlation

Pure Gamma-Gamma Cascade

Consider a cascade $A \rightarrow B \rightarrow C$ with both gamma rays of pure multipole order L_1 and L_2 respectively. As previously discussed, the directional correlation function can be written as

$$W(\theta) = \sum_{k \text{ even}} \alpha_k P_k(\cos \theta) \quad , \tag{6}$$

where

$$k_{max} = \text{Min.}(2I_b, 2L_1, 2L_2) \ .$$

This selection rule on k_{max} was derived by Yang.[31] In practice k is no larger than 4. The coefficients α_k are equal to the product of two factors, with each factor depending on one of the gamma transitions. Thus,

$$\alpha_k = \alpha_k^{(1)} \alpha_k^{(2)} \quad , \tag{7}$$

where

$$\begin{aligned} \alpha_k^{(1)} &= F_k(L_1 L_1 I_a I_b) \\ \alpha_k^{(2)} &= F_k(L_2 L_2 I_c I_b) \ . \end{aligned} \tag{8}$$

The F coefficients have been tabulated by Ferentz and Rosenzweig.[32]

Mixed Gamma-Gamma Cascade

A gamma ray has mixed multipolarity if it must be described by more than one value of angular momentum. Ling and Falkoff[25] first treated the directional correlation for a cascade with one gamma ray of mixed multipolarity. The analysis of gamma-gamma directional correlations envolving multipole mixtures has been discussed by Arns.[13,33]

Consider a gamma ray of mixture L and L + 1. Let δ be the ratio of the reduced matrix elements for L + 1 radiation to L radiation.

Then δ^2 is the intensity ratio of the L + 1 radiation to L radiation. Since the reduced matrix elements are real, δ is real.

For mixtures in both gamma transitions of L_1, $L_1 + 1$ and L_2, $L_2 + 1$, the function $W(\theta)$ still has the form of Equation (6), with

$$k_{max} = \text{Min.}[2I_b,\ 2(L_1 + 1),\ 2(L_2 + 1)] \tag{9}$$

and

$$\alpha_k^{(1)} = F_k(L_1,L_1,I_a,I_b) + 2\delta_1 F_k(L_1,L_1 + 1,I_a,I_b) + \delta_1^2 F_k(L_1 + 1,L_1 + 1,I_a,I_b). \tag{10}$$

The expression for $\alpha_k^{(2)}$ may be obtained by replacing L_1 with L_2, δ_1 with δ_2, and I_a with I_c.

The experimental data is usually put in the form

$$W'(\theta) = 1 + B_2A_2P_2(\cos\theta) + B_4A_4P_4(\cos\theta), \tag{11}$$

where

$$A_k = \frac{\alpha_k^{(1)}}{\alpha_o^{(1)}} \frac{\alpha_k^{(2)}}{\alpha_o^{(2)}}$$

The experimental function $W'(\theta)$ differs from the theoretical function $W(\theta)$ due to the attenuation factors B_k, which depend on the geometry of the experiment.

Let Q_ν be the fraction of the ν-th gamma ray with multipolarity of L + 1. Then

$$Q_\nu = \frac{\delta_\nu^2}{1 + \delta_\nu^2} \quad , \tag{12}$$

and $A_k^{(\nu)}$ can be put in the form

$$A_k^{(\nu)} = a_k^{(\nu)}(1-Q_\nu) + b_k^{(\nu)}\sqrt{Q_\nu(1-Q_\nu)} + c_k^{(\nu)}\,Q_\nu \quad , \tag{13}$$

where $a_k^{(\nu)}$, $b_k^{(\nu)}$, and $c_k^{(\nu)}$ correspond to appropriate F coefficients for the cascade.

If one transition, say the first, is a mixture of dipole and quadrupole radiation, and the other transition is pure, then

$$A_2 = A_2^{(1)}A_2^{(2)} = \{a_2^{(1)}(1-Q_1) + b_2^{(1)}[Q_1(1-Q_1)]^{1/2} + c_2^{(1)}Q_1\}\, a_2^{(2)} \qquad (14)$$

$$A_4 = A_4^{(1)}A_4^{(2)} = c_4^{(1)}Q_1 a_4^{(2)} \qquad (15)$$

The equation of $A_2^{(1)}$ is an ellipse when plotted as a function of Q_1, and $A_4^{(1)}$ versus Q_1 is a straight line. Such curves have been plotted for all useful spin assignments.(34)

The experimental data yield $A_2^{exp.} \pm \sigma_2$ and $A_4^{exp.} \pm \sigma_4$, where σ_2 and σ_4 are the mean square errors. If these coefficients are divided by $A_2^{(2)}$ and $A_4^{(2)}$, respectively, the results may be compared to the theoretical $A_2^{(1)}$ and $A_4^{(1)}$ curves.

For a mixture in both transitions, the $A_4^{(\nu)}$ each equal $c_4^{(\nu)}Q_\nu$, and the $A_2^{(\nu)}$ each have the form of Equation (13). Using the relationship

$$A_2^{exp} \pm \sigma_2 = A_2^{(1)}A_2^{(2)} \quad , \qquad (16)$$

a plot of $A_2^{(1)}$ versus $A_2^{(2)}$ may be made. The result for the experimental values included within the error limits is an area bounded between two hyperbolae. Then the various theoretical curves for $A_2^{(1)}$ versus Q_1 and $A_2^{(2)}$ versus Q_2 may be compared with the experimental data. In order to make a unique assignment, additional information, such as quadrupole contents from internal conversion data, is needed.

CHAPTER IV

EXPERIMENTAL TECHNIQUES

Introduction

Many techniques are available to the experimenter in studying radioactive nuclei. In the present investigation the transitions connecting the nuclear energy levels were studied by observation of gamma-ray spectra and by means of internal conversion, coincidence, and directional correlation measurements.

In coincidence and directional correlation measurements, coincidences between gamma rays are recorded. In addition to real coincidences of gamma rays emitted from the same nucleus, there will be accidental coincidences of gamma rays originating from different nuclei. The real coincidence rate, N_R, is given by

$$N_R = N_E - N_A \quad , \tag{1}$$

where N_E is the experimental coincidence rate and N_A is the accidental coincidence rate. The real coincidence rate can also be expressed as

$$N_R = N\sigma_1\epsilon_1\sigma_2\epsilon_2 \, , \tag{2}$$

where N is the source strength, σ_1 and σ_2 are the solid angles subtended by the detectors in relation to the source, and ϵ_1 and ϵ_2 are the detector efficiences.

The accidental coincidence rate is a function of the coincidence circuit resolving time, τ, which indicates how closely two pulses must be spaced (in time) in order to be recorded as a coincidence. The accidental

coincidence rate is given by

$$N_A = 2\tau N_1 N_2 \quad , \tag{3}$$

where N_1 and N_2 are the counting rates for the two detectors. Since $N_1 = N\sigma_1\epsilon_1$ and $N_2 = N\sigma_2\epsilon_2$, then

$$N_A = 2\tau N^2\sigma_1\epsilon_1\sigma_2\epsilon_2 \quad . \tag{4}$$

The accidental coincidence rate may be experimentally determined by separating the two detectors and putting a source in front of each one.

Dividing Equation (2) by Equation (4), the following expression is obtained:

$$\frac{N_R}{N_A} = \frac{1}{2\tau N} \quad .$$

This ratio should be kept as large as possible in order to have a small accidental correction for the experimental data. The desired result may be achieved by using a small τ or N. However, N must be large enough so that the real coincidence rate is adequate and the experiment can be done in a reasonable amount of time.

A lower limit on τ is set by the properties of the detecting crystal. It can be shown that the resolving time should not be less than the scintillation decay time if the energy information is to be maintained.[35] For NaI(Tl) crystals this imposes a lower limit of 2.5×10^{-7} sec. on the resolving time.

Shorter resolving times may be achieved with the loss of energy information. This is the basis of a "fast-slow" coincidence circuit. In such a circuit each pulse is fed into a "slow" channel for energy selection and into the "fast" coincidence circuit. The outputs

of the slow channels and the fast coincidence circuit are then brought together in a coincidence circuit. In order to obtain satisfactory operation of the fast coincidence circuit, the pulses feeding the circuit must be uniform, have a fast rise, and have a short duration. In accomplishing this, all energy information is lost.

Directional Correlation Measurements

Directional Correlation Apparatus

A fast-slow coincidence circuit was used in the directional correlation measurements. The main features of the circuit were designed by Scharenberg[36] and Stewart[35], and modifications were made by Arns.[37] A block diagram of the apparatus is shown in Figure 3. The individual parts will be described in the following sections.

Detectors

The detectors consisted of 2-in. diameter by 2-in. thick NaI(Tl) crystals mounted on RCA 6342A phototubes. The crystals were coupled to the phototubes with Dow-Corning 200 Fluid (viscosity = 10^6 cs.). Each phototube was surrounded by mu-metal for magnetic shielding and by a 3-in. diameter iron pipe, with the crystal projecting through a cap.

Teflon beta shields were used on the crystal fronts. Cylindrical lead shields around the crystals and extending one inch in front of the crystals were used in order to reduce scattering from surrounding objects.

Fast Coincidence Circuit

The output pulses from the cathode follower after the phototube are fed into a series of amplifiers with band widths of 100 megacycles.

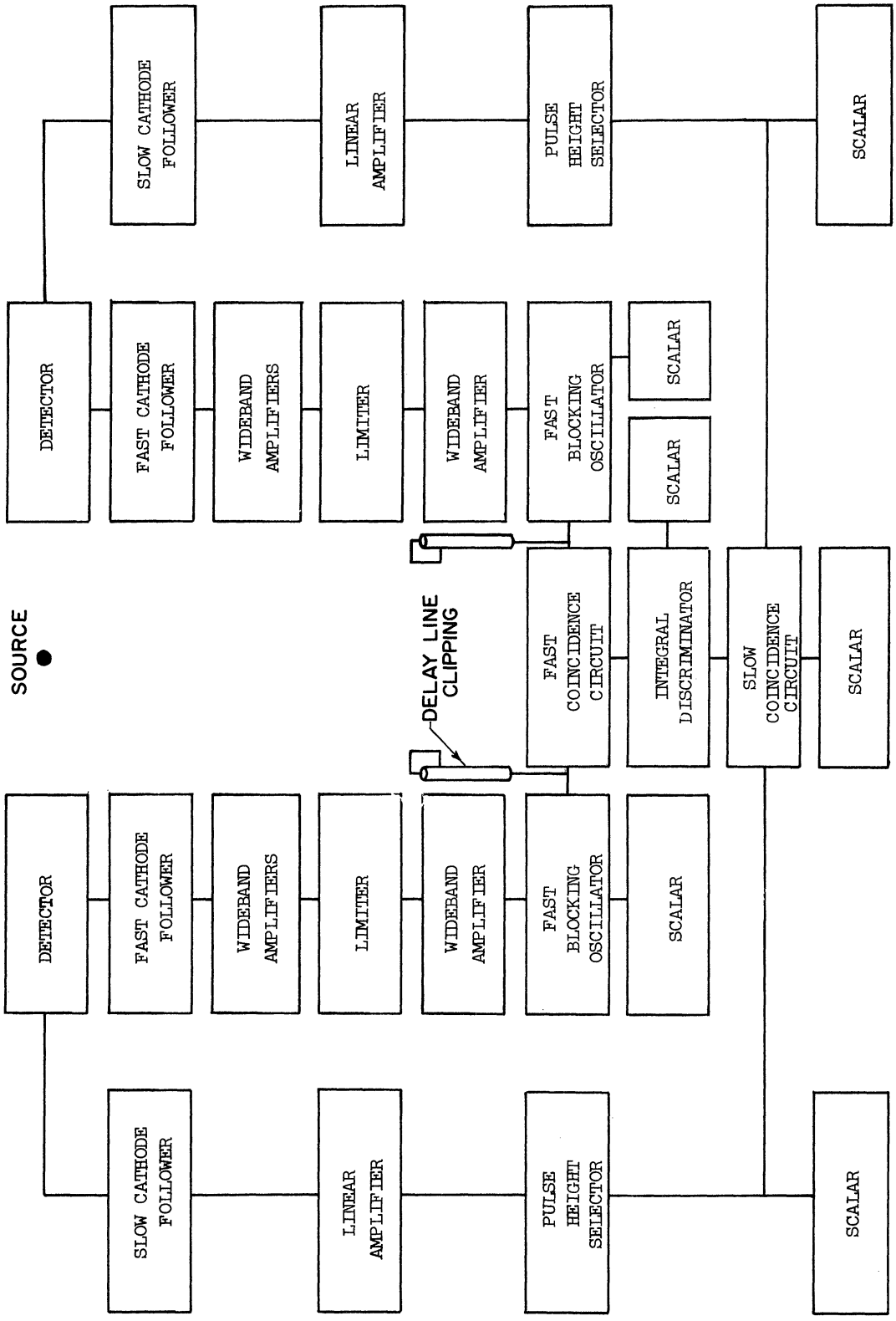

Figure 3. Fast-Slow Coincidence Apparatus Used in the Directional Correlation Measurements.

After passing through a limiter, the pulses are again amplified by a wideband amplifier. The pulses are then fed into a fast blocking oscillator. Delay line clipping is used to shorten the pulse to 20×10^{-9} sec. Such pulses from both phototubes are fed into a Garwin type coincidence circuit.[38,39] A discriminator after the coincidence circuit allows only the coincident pulses to pass. The resolving time for the Eu^{153} cascade measurements was 20 millimicroseconds. A slightly different circuit with a resolving time of 50 millimicroseconds was used in the Eu^{155} cascade measurement. A variable delay line in one channel may be adjusted so that pulses from coincident gamma rays reach the two inputs of the coincidence circuit at the same time. Changing the length of cable in one channel has the same effect.

Energy Selection

The phototube pulses are also fed into slow channels which are used for energy selection. After passing through a cathode follower, the pulses are fed into a linear amplifier and then into a pulse-height selector of the Johnstone[40] type, modified by Lu.[41] The pulse-height selector gives a uniform output pulse for every input pulse which falls in a selected energy range.

Since the gamma rays frequently are not resolved, the pulses selected in such a manner often originate from more than one transition. The Compton distribution of higher energy transitions also causes interference.

Slow Coincidence Circuit

The pulses from the fast coincidence circuit and the two energy selection circuits are brought together in a triple coincidence circuit which gives an output pulse only if all three input pulses coincide. Thus, the energy and time information of the pulses are combined. The input pulses trigger univibrators which give uniform pulses of one microsecond duration. These pulses are then fed into a diode-type coincidence circuit.[42] A discriminator allows only the coincident pulses to pass.

Recording

Scalars are used to record the number of pulses after each blocking oscillator in the fast channels, after each pulse height selector in the slow channels, after the fast coincidence circuit, and after the slow coincidence circuit.

Source Preparation

It was pointed out in Chapter III that a correlation may be attenuated if the radioactive source is not in the proper environment. The sources used in the present research were dissolved in dilute nitric acid.

The source holders were made from lucite. The cavity for the source was about 0.3 cm in diameter, 1.2 cm high, and had a wall 0.02 cm thick. The cavity was capped and supported on a thin lucite rod.

Photoelectric absorption of gamma rays can take place in the source. This effect produces an anisotropic distribution of coincidences.

Therefore, the source holder should contain a small diameter cavity and the solution should be weak, particularly for a source of high atomic number. Scattering effects are also possible and can be likewise reduced by using a small cavity with a thin wall. In the present experiment these errors were negligible.

Collection of Data

The data were collected by observing the coincidence rate as a function of angle. One detector was kept in a fixed position, and the second detector was rotated about the centrally placed source. The detectors were 10 cm from the source, except in the Eu^{155} cascade, where one detector was at 7 cm.

Since the coincidence rate can be expressed in even powers of the Legendre polynomials, all of the necessary information can be obtained in one quadrant. However, two quadrants are commonly used in order to correct for certain errors which will be explained below.

The data in these measurements were taken from 90° to 270°. Each run for the Eu^{153} cascade consisted of taking data for five minute periods at seven angles in each quadrant. Many such runs yielded a sufficient number of coincidences at each angle. Due to the shorter half-life of the Sm^{155}, a run for the Eu^{155} cascade was for two minute periods at five angles in each quadrant.

In making an analysis the data for the corresponding angles in the two quadrants are combined. This reduces errors caused by a slightly off-centered source or scattering from nearby objects. In addition, the double quadrant sequence makes half-life corrections

negligible, provided the half-life of the isotope is longer than the length of one run. Because of the number of runs, short-term instabilities tend to average out.

Interpretation of Data

After correcting the data for accidental coincidences, the corresponding data from all of the runs were added. In the case of the Eu^{155} cascade, corrections were made for the half-life. After making a least squares fit,[43] the coefficients were normalized to the form:

$$W'(\theta) = 1 + B_2A_2P_2(\cos\theta) + B_4A_4P_4(\cos\theta),$$

where B_k are geometrical attenuation coefficients. The experimental A_k are interpreted in the manner discussed in Chapter III.

Geometrical Corrections

The detectors must be sufficiently large in order to obtain an adequate counting rate and perform the experiment in a reasonable time. However, detectors of a finite size measure coincidences between two gamma rays over a range of angles, and not at just one angle. This results in an attenuation of the correlation. The finite size of the detector leads to a similar effect.

Several methods can be used to obtain the attenuation coefficients, B_k. Rose[43] has calculated the coefficients as a function of the absorption coefficient for a point source incident on a cylindrical scintillation crystal. Lawson and Frauenfelder[44] used experimentally determined angular efficiency curves in determining the correction for a similar

situation. Church and Kraushaar[45] used annihlation radiation to measure the corrections for gamma rays near 511 kev. Feingold and Frankel[46] have studied corrections for detectors with arbitrary shapes and for axially extended sources. Their theoretical results have been used in determining the experimental attenuation coefficients as functions of the transition energy and the cylindrical source length for source to crystal distances of 7 cm and 9.9 cm.[47] In this determination the efficiency of a 2-in. x 2-in. NaI(Tl) crystal was observed as a function of angle for a collimated gamma-ray beam of a certain energy. The procedure was repeated for various energy gamma rays. The B_k found in this way for 511 kev agree remarkably well with the determination of Church and Kraushaar.[45]

Coincidence Measurements

Coincidence Apparatus

A block diagram of the apparatus used in the coincidence measurements is shown in Figure 4. The apparatus is a modification of that used in the directional correlation on the Eu^{155} cascade.

As in the directional correlation measurements, a fast coincidence circuit is used in order to obtain a good resolving time. The fast coincidence circuit had a resolving time of 50 millimicroseconds for the coincidence measurements in Eu^{155} and 30 millimicroseconds for the measurements in Eu^{153}. A pulse-height selector is used after one of the detectors in order to select gamma rays which fall in a certain energy range. Pulses from the fast coincidence circuit and the pulse-height selector are fed into a double coincidence circuit similar to the slow coincidence circuit discussed previously. The output of the double coincidence circuit feeds a linear gate,

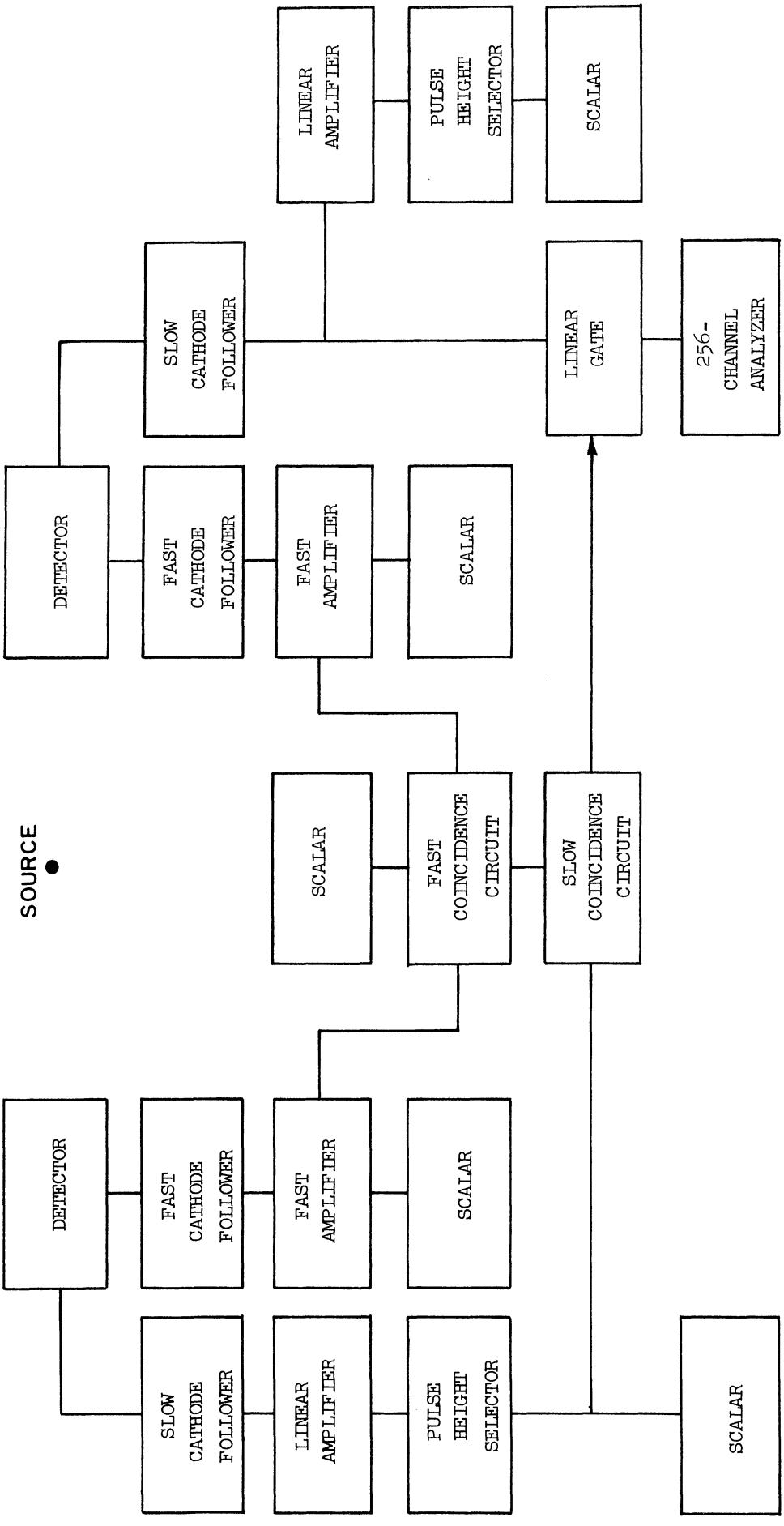

Figure 4. Fast-Slow Coincidence Apparatus Used in the Coincidence Measurements.

and allows pulses from the second detector to be passed. The energy information is retained in the pulses which pass through the gate circuit. Thus, pulses from the second detector which are coincident with pulses in a selected energy range from the first detector are allowed to pass through the linear gate circuit. These pulses are analyzed according to their energy in a 256-channel analyzer. The linear amplifier, pulse height selector, and scalar shown on the right-hand side of Figure 4 are used for normalization of counting rates between accidental and coincidence spectra.

The circuit for the linear gate is shown in Figure 5. Pulses from one phototube pass through a preamplifier before reaching the gate circuit. The trigger pulse from the double coincidence circuit passes through a pulse transformer so that the necessary positive and negative pulses may be obtained. The gate circuit consists of six diodes and is described by Millman and Taub.[48] When a trigger pulse occurs, the two diodes at the trigger-pulse inputs are back biased, and current flows through the remaining four diodes due to the $\pm$ 24 volts. Then the pulse from the phototube is allowed to pass. Otherwise, the $\pm$ 8 volts clamps the voltages at P_1 and P_2 so that the remaining four diodes do not conduct.

Collection of Data

The detectors faced each other and were 2.54 cm from the source in most measurements. A Compton shield of 6.4 mm Pb surrounded by 0.8 mm Cd and 0.4 mm Cu was used to reduce scattering. This is necessary, since a gamma ray is often partially absorbed in one crystal by the Compton effect. The scattered radiation can then be recorded as a coincidence in the second detector.

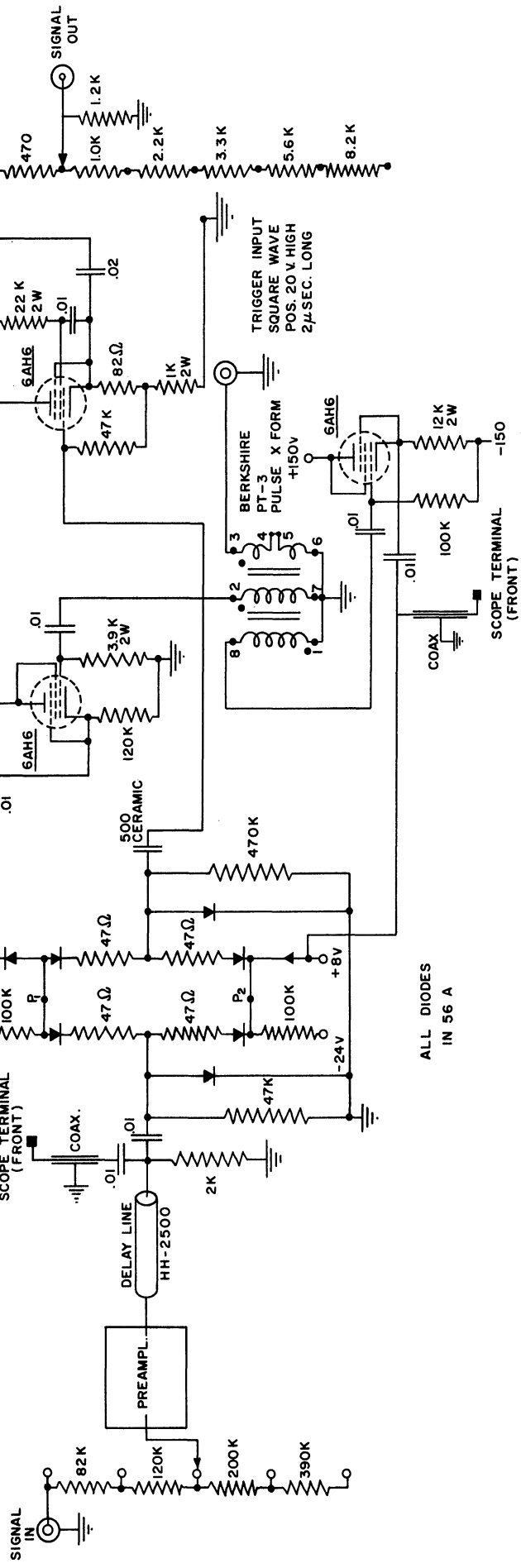

Figure 5. Linear Gate Circuit Used in the Coincidence Measurements.

In all cases accidental spectra were subtracted from the observed spectra to obtain the spectra shown.

Well-Crystal Spectra

Another method used in coincidence measurements envolves the use of a well crystal. A weak source is placed in a small cylindrical hole leading to the center of a NaI(Tl) crystal. Two gamma rays in cascade will both be detected simultaneously in the crystal. The resulting pulse will have an amplitude corresponding to the sum of the two gamma-ray energies. A comparison of such a spectrum with a spectrum taken with the source at a distance from the crystal will show an enhancement of the sum peak in relation to the peaks of the individual transitions. A weak source must be used so that accidental summing of gamma rays from different nuclei will not occur to a significant extent.

Internal Conversion Measurements

A nucleus may lose its excitation energy through gamma radiation. Internal conversion represents an alternative mode of decay. In this process nuclear energy is transferred to one of the atomic electrons, which is subsequently ejected from the atom with a kinetic energy E_e given by $E_e = E_o - E_b$, where E_b is the binding energy of the ejected electron and E_o is the available energy of decay, which corresponds to the competitive gamma-ray energy. The ejected electrons travel in a circular path with a radius dependent on their energy and the field strength. The detector used in the present analysis was a photographic plate. A linear source is used so that electrons of the same energy moving perpendicular to the

field form a line on the plate. The energy of the electrons is determined from their radius and the field strength.

Internal conversion is an important experimental tool because the energy of a transition may be accurately determined. The resolution of the spectrometer was about 0.5%. In comparison, the resolution of a NaI(Tl) crystal is about 10% for 662 kev. The improved resolution also aids in observing weak transitions which are near strong ones.

The K-shell internal conversion coefficient of a transition is defined as the ratio of the number of K-shell electrons to the number of gamma rays emitted. The total internal conversion coefficient is the sum of the coefficients for all of the shells. Theoretical internal conversion coefficients have been calculated by Rose[49] and by Sliv and Band.[50]

A variable-field magnetic spectrometer was used in the Sm^{155} internal conversion measurements. The spectrometer has a fast-entry feature so sources can be changed rapidly. The sources consisted of about 1 mg/cm^2 of powder mounted on a piece of Scotch tape about 0.8 cm wide. The tape was attached to a polystyrene frame. Identical sources were used so one source could be irradiated while the second source was in the camera.

CHAPTER V

THE LEVEL STRUCTURE OF Eu^{153}

Introduction

The beta decay of the 47-hour Sm^{153} to Eu^{153} and the electron capture decay of the 225-day Gd^{153} to Eu^{153} have been studied by a number of investigators.[51-75] Figure 6 shows the decay scheme given by McCutchen[51]

There is general agreement about the levels at 84 kev, 97 kev, 103 kev, 172 kev, and 187 kev. The 70-kev gamma ray has been observed in coincidence with the 103-kev gamma ray in the decay[60] of Sm^{153} and in the decay[51] of Gd^{153}; both transitions[75] are M1 + E2. The 97-kev gamma ray was first observed by Church and Goldhaber[66] by means of internal conversion measurements on Gd^{153}. This transition[51,71,72] is strongly fed in the decay of Gd^{153}. Recently, Walters et al.[65] observed a 97-kev transition with a bent-crystal spectrometer in the Sm^{153} decay with an intensity of less than 5% of the 103-kev gamma ray. The levels at 84 kev and 187 kev, and the corresponding gamma transitions have been observed by Coulomb excitation.[76-78]

The energies of the strong beta components in the Sm^{153} decay have been measured as 803 kev, 698 kev, and 640 kev.[54,58,60,61,63] The 698-kev beta transition has been observed in coincidence with the 103-kev gamma ray, and the 640-kev beta ray has been observed in coincidence with gamma transitions of 70 kev, 103 kev, and 173 kev.[54,58,60]

The half-life of the 103-kev level has been measured as 4×10^{-9} sec.,[54,56,74] and the 173-kev level has a half-life of 0.14×10^{-9} sec.[54] McGowan[56] observed that the 97-kev gamma ray

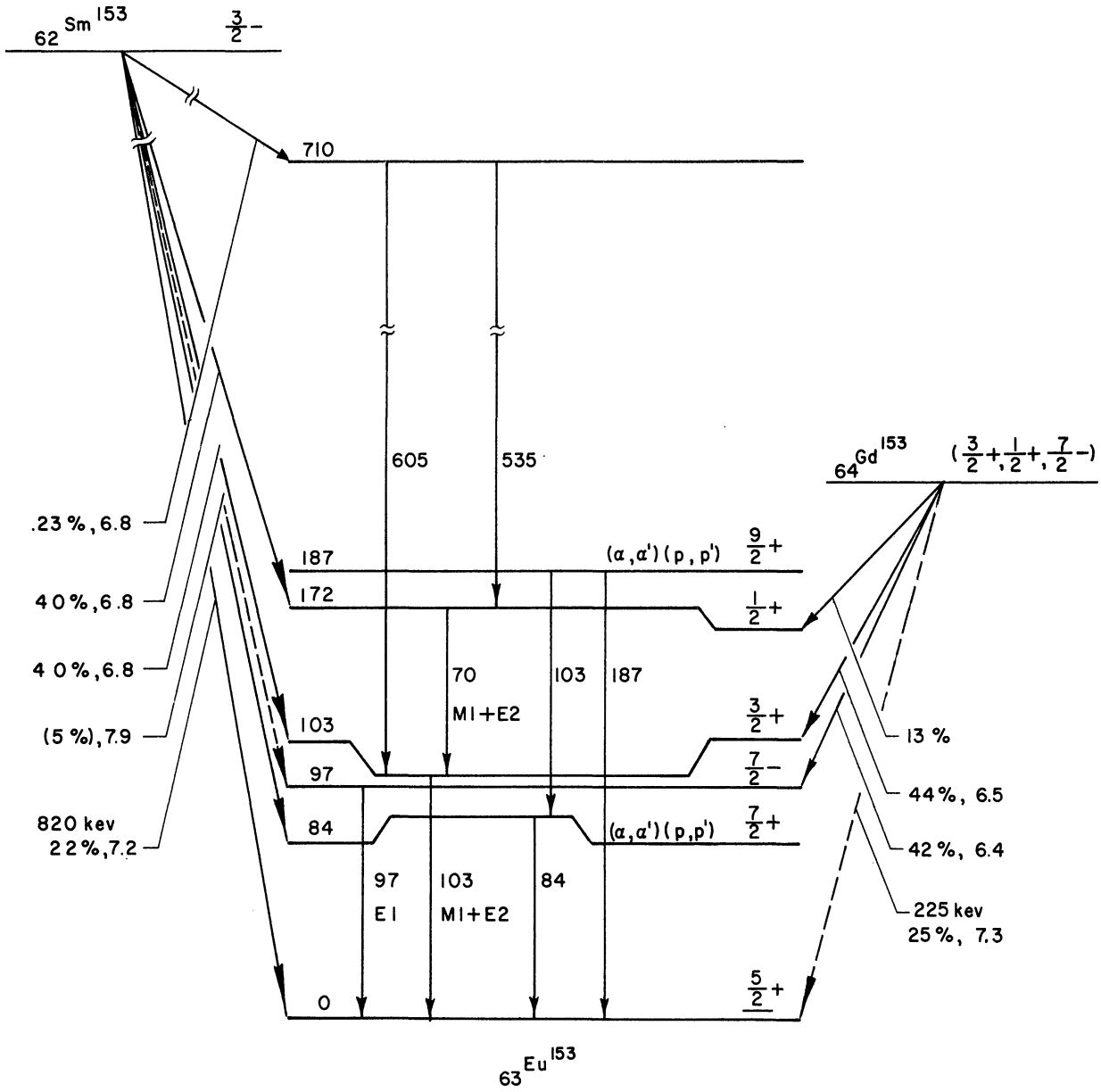

Figure 6. Decay Scheme of Sm^{153} and Gd^{153}, Due to McCutchen.[51] The energies are in kev. The numbers after the intensities are log ft values.

is in prompt coincidence with the K-capture x-rays from Gd^{153}. Vergnes[74] obtained a half-life of $\leq 10^{-9}$ sec. for this level.

There has been uncertainty over the positions in the decay scheme of the 535-kev and 605-kev transitions from the Sm^{153} decay. Dubey et al.[60] and McCutchen[51] observed that the 103-kev transition and probably the 70-kev transition are in coincidence with the 535-kev transition. The 103-kev transition was observed to be in coincidence with the 605-kev transition by Dubey et al.[60]

Some disagreement also exists over the internal conversion coefficients and the relative intensities of the transitions. Thus, the present coincidence and angular correlation measurements were undertaken in order to resolve some of the previous uncertainties and to study the level structure more completely.

Experimental Procedure

Samples of very pure, natural samarium oxide were dissolved in nitric acid and irradiated in a flux of 2×10^{12} neutrons/cm^2/sec for periods of seven hours in the Ford Nuclear Reactor. Measurements were taken within a period of three and ten days after irradiation. This allowed the 22-minute Sm^{155} and 9.3-hour Eu^{152m} to decay. Immediately after irradiation the 842-kev gamma ray in Eu^{152m} had an intensity of about one-half of the 610-kev transition in Sm^{153}. The half-life of Sm^{153} was followed for 32 days, and only these short-lived impurities were observed.

A sample of gadolinium oxide enriched to 36.2% in Gd^{152} was irradiated for 64 hours in the Ford Nuclear Reactor. Measurements were begun 36 days after the completion of irradiation in order to allow the short-lived Gd activities to decay. The only observed impurities were Eu^{152} and Tb^{160}. The 244-kev gamma ray in Eu^{152} and the 298-kev gamma ray in Tb^{160} each had an intensity of about 8% of the 173-kev transition in Gd^{153}.

All of the transitions observed in the Sm^{153} coincidence measurements decayed with the proper half-life. In all cases the accidental spectra were small and were subtracted from the curves shown. The x-ray, 81-kev, 160-kev, and 355-kev gamma rays in Ba^{133} and the 511-kev transition from Na^{22} were used in calibrating the energy in the coincidence measurements.

Results for Sm^{153} Decay

Gamma-Ray Spectra

Figure 7 shows gamma ray spectra from the Sm^{153} decay as recorded on a 256-channel analyzer. The spectrum shown in Figure 7A was taken with a teflon beta shield; a weak source was used at 64 cm from the crystal in order to avoid accidental and real summing of gamma rays in the region of 173 kev. A weaker source at 100 cm from the crystal showed the 173 kev transition better resolved. In order to obtain better statistics on the high energy radiations, the spectrum shown in Figure 7B was taken with a strong source at 5.7 cm from the crystal with suitable absorbers. Spectra of Na^{22} and Cs^{137} were taken with the same geometry and absorbers used for

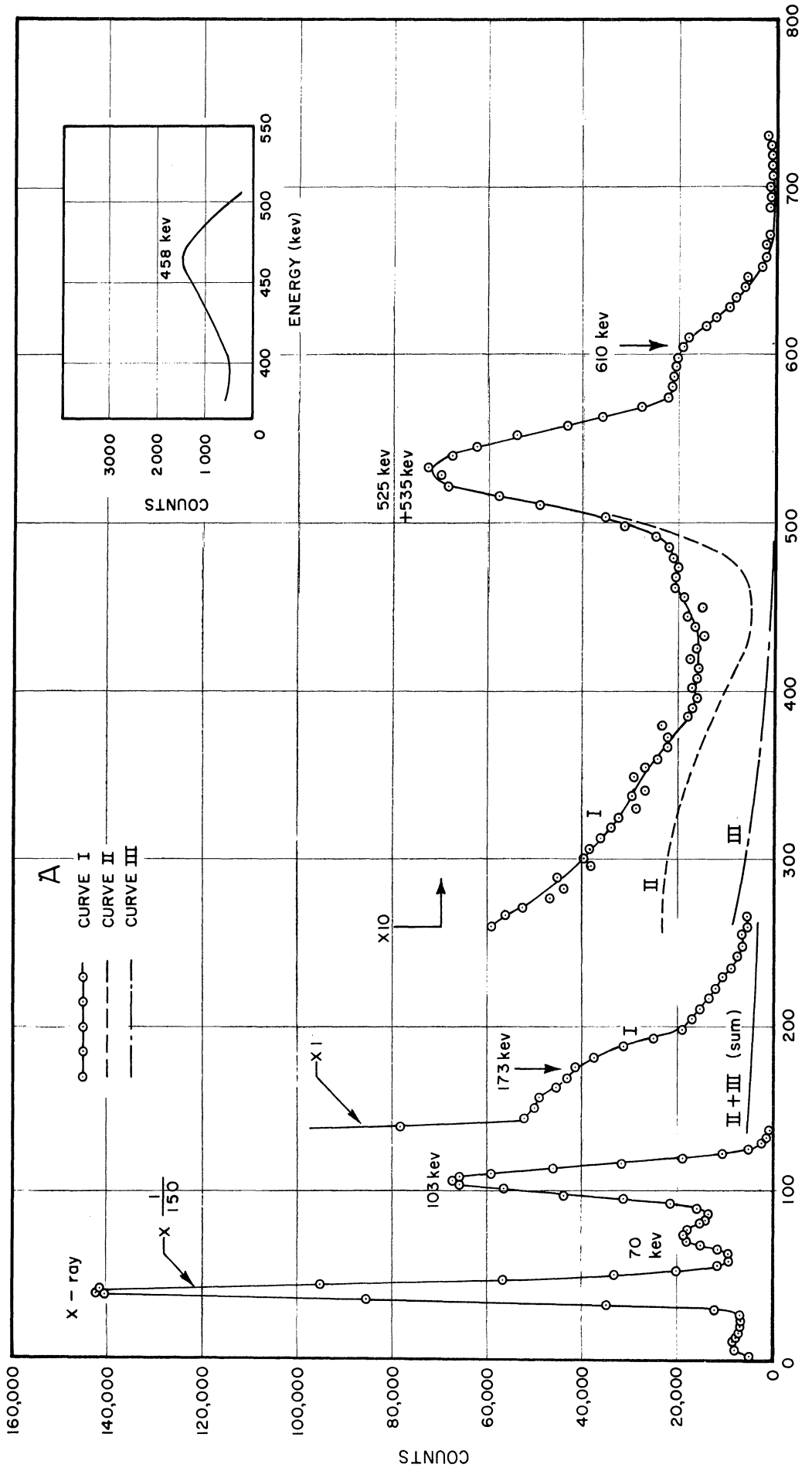

ENERGY (kev)

Figure 7A.

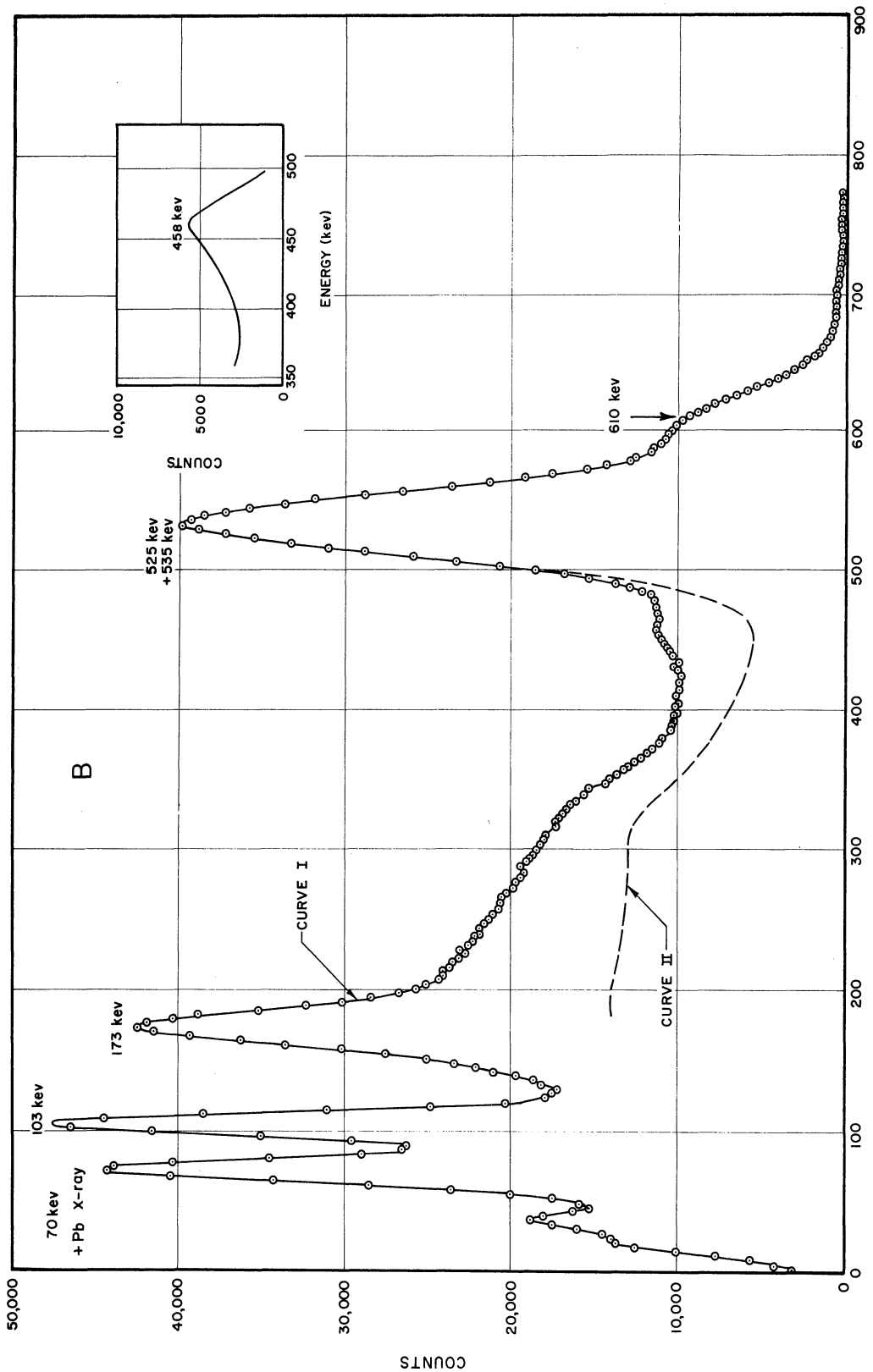

Figure 7B. Scintillation spectra of gamma rays in the decay of Sm^{153}. Curve AI is with the Sm^{153} source at 64 cm from the crystal and with a 6.5 mm feflon beta shield. Curve BI is with the Sm^{153} source at 5.7 cm from the crystal and with absorbers of 0.084 cm Pb, 0.013 cm W, and 0.203 cm Cd. Curves AII and BII are the photoelectric and Compton distributions for the gamma rays which are in ghe regions of 530 kev and 610 kev. Curve AIII is the theoretical internal Bremsstrahlung. The inserts in A and B show the spectra in the 458-kev region, after subtracting the spectra for the higher energy radiations and the internal Bremsstrahlung.

Sm^{153} in Figure 7A and 7B. From these data the photoelectric and Compton distributions were determined for the gamma rays which are in the regions of 530 kev and 610 kev.

The theoretical internal Bremsstrahlung was calculated in order to determine its effect in the region above 173 kev, where the gamma transitions are very weak. The result is shown in Figure 7A.

Both spectra in Figure 7 indicate a transition of about 458 kev in addition to the gamma transitions previously reported.

The iodine x-ray escape peak from the 103-kev gamma ray is in the region of the 70-kev transition. In order to determine the intensity of the escape peak, spectra of the 103-kev transition in Se^{81m} were taken after the weak transitions in the 18-minute Se^{81} had decayed for about 200 minutes. The Se used for irradiation was enriched to 97% in Se^{80}. After subtracting the very weak Compton distribution due to high energy radiations, these spectra were compared with Sm^{153} spectra taken with the same geometry and at the same time as the Se^{81m} spectra. A frontal shield of 6.5 mm teflon was used in all cases. The spectra are shown in Figure 8. Corrections were made for absorption, crystal efficiency, and iodine x-ray escape. The relative intensity of the 70-kev gamma ray to the 103-kev gamma ray was calculated to be 0.12 ± 0.03 and 0.13 ± 0.03 at source to crystal distances of 2.54 cm and 10.2 cm respectively.

Background was subtracted from all spectra. All parts of the Sm^{153} spectra decayed with a 47-hour half-life.

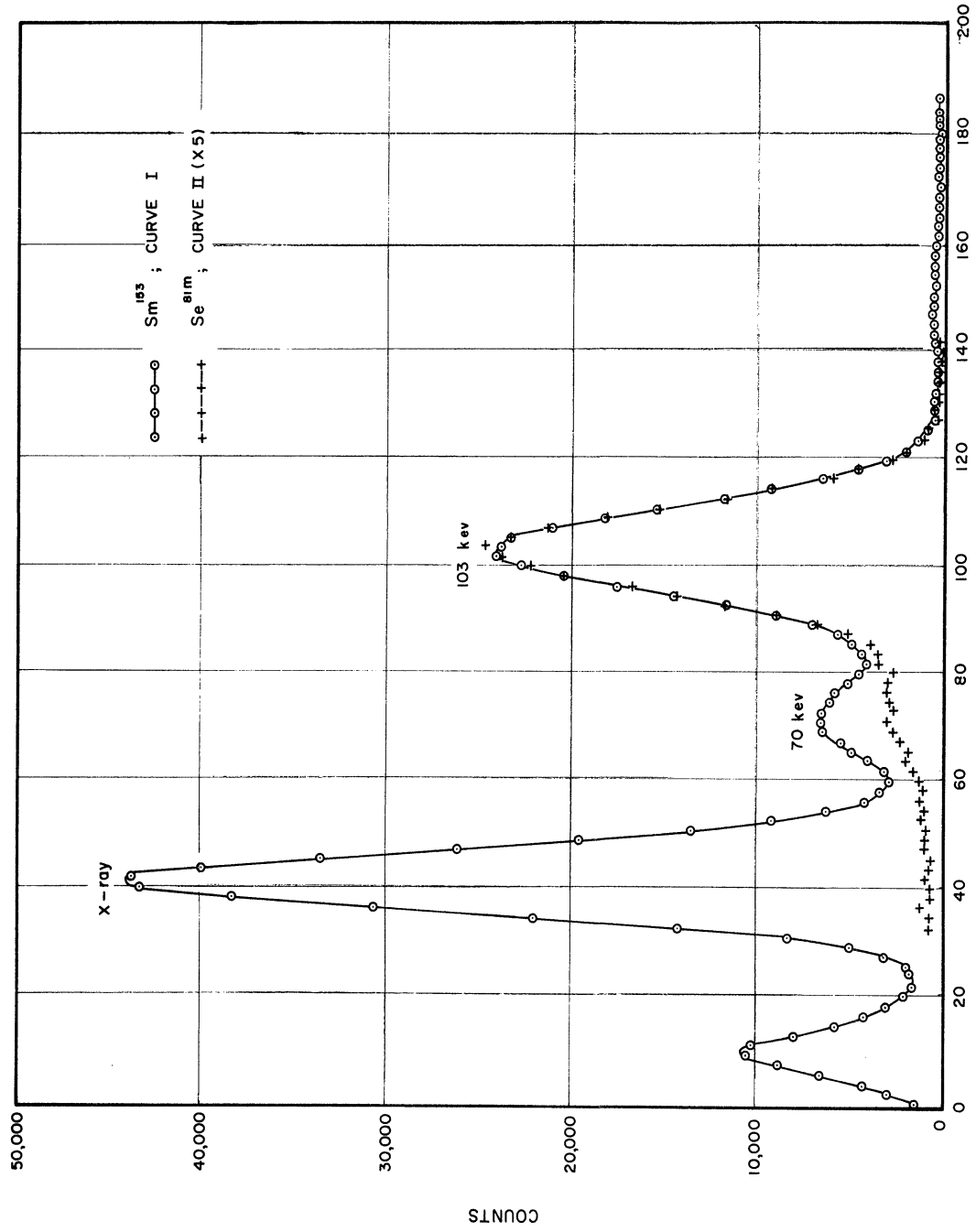

Figure 8. Curve I is Scintillation Spectrum of Gamma Rays in Decay of Sm^{153}. The peak at 12 kev is due to the iodine x-ray escape for the Eu x-ray. Curve II is scintillation spectrum of gamma rays from decay of Se^{81m}. Both spectra were taken at a source to crystal distance of 2.54 cm.

Coincidence Measurements

Figure 9 illustrates the spectrum of gamma rays in coincidence with the 103-kev transition (89-kev to 116-kev range) from Sm^{153}. The decreased intensity ratio of the 535-kev transition to the 610-kev transition in comparison with the singles spectrum indicates that there is another transition near 535 kev whose intensity is 30 ± 10% of the combined intensity. This coincidence run was repeated with the gain of the multichannel analyzer raised. The resulting data, shown in Figure 10, were used to calculate α_k for the 70-kev gamma ray.

The spectrum of gamma rays coincident with the 173-kev gamma ray (166-kev to 191-kev range) is shown in Figure 11. Shielding was used in front of both crystals to attenuate the low energy radiations. Coincidences are shown with gamma rays of 154 kev, 352 kev, and 422 kev. The possibility of the 154-kev transition coming from summing of low energy transitions was eliminated due to the small number of coincidences at low energies. As will be seen below, this gamma ray along with the peak at 525 kev are mostly due to interference.

The spectra of coincidences with the 500-kev to 540-kev range and with the 612-kev to 665-kev range are shown in Figure 12. These spectra were taken consecutively and are approximately normalized in the 100-kev region. Calibration lines in the coincidence spectra of Ba^{133} showed that there were no energy shifts during the coincidence runs. The 103-kev gamma ray is shown to be in coincidence with the 535-kev transition. A weak coincidence at 154 kev is also shown. No 70-kev coincidence is indicated. The 97-kev gamma ray is in coincidence with the 610-kev transition. This conclusion is supported by the weaker x-ray on this spectrum.

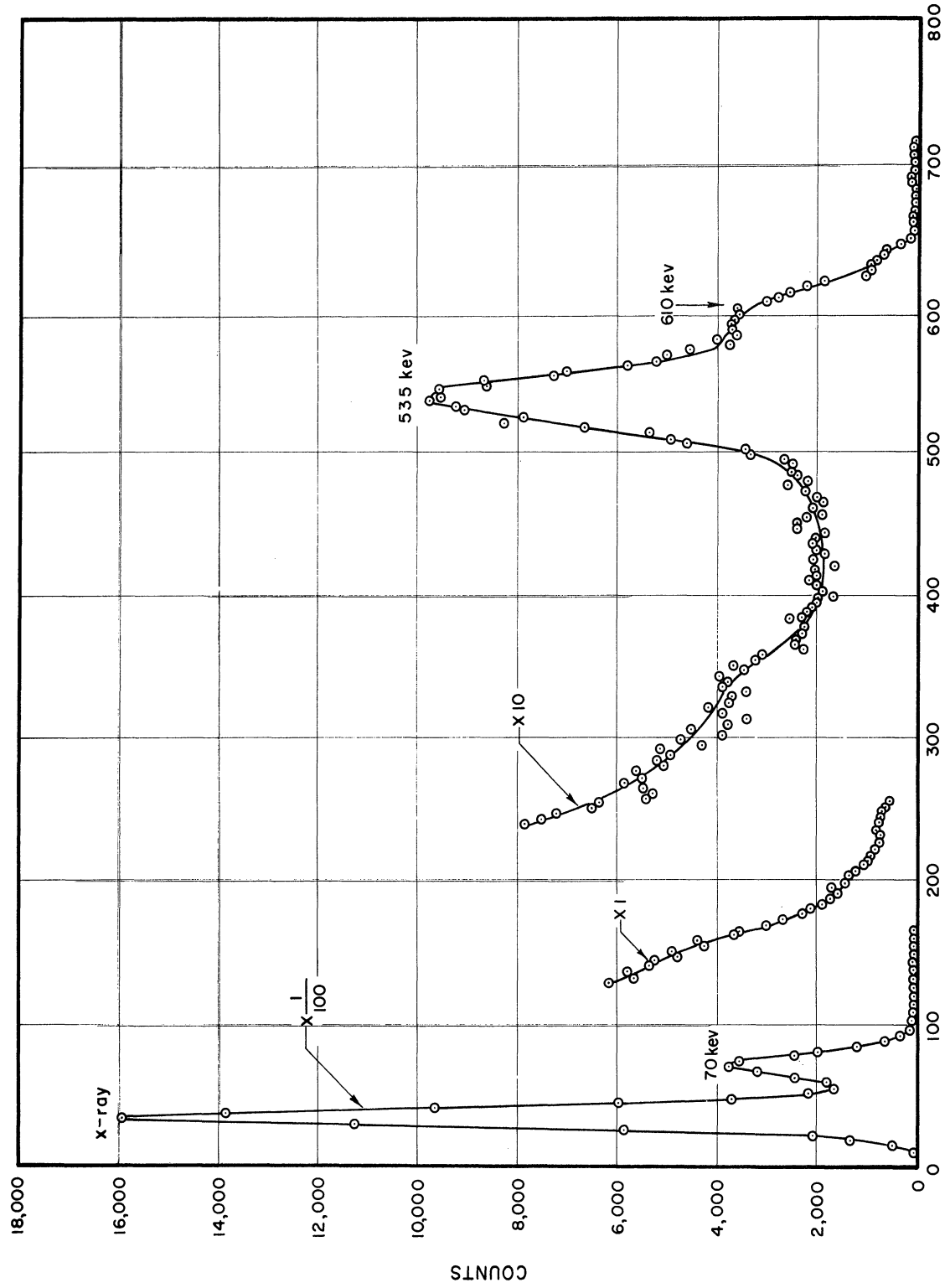

Figure 9. Spectrum of Gamma Rays in Coincidence with 103-kev Gamma Ray (89-kev to 116-kev range) in Decay of Sm^{153}.

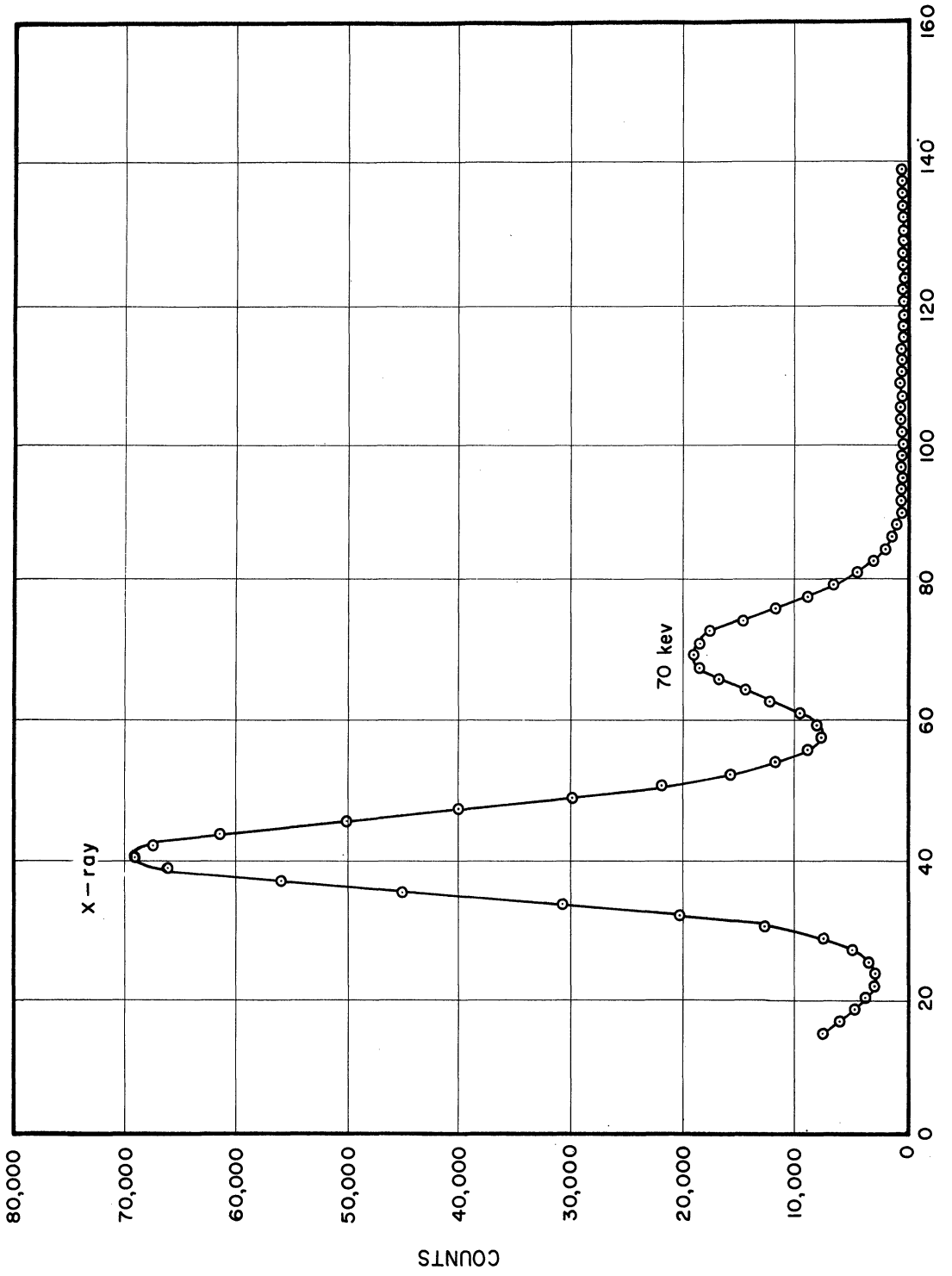

Figure 10. Spectrum of Gamma Rays in Coincidence with 103-kev Gamma Ray in Decay of Sm^{153}.

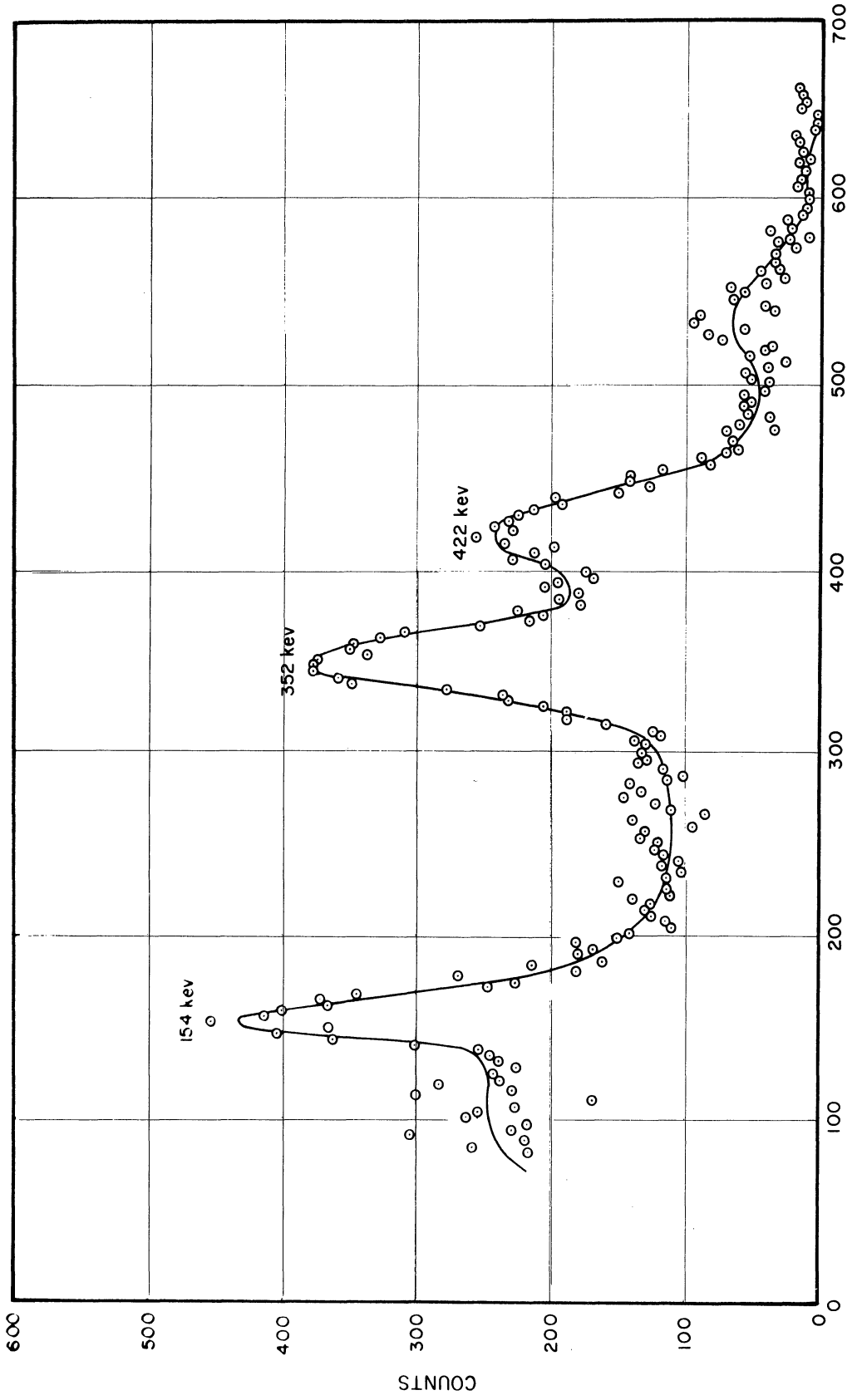

Figure 11. Spectrum of gamma rays in coincidence with 173-kev gamma ray (166-kev to 191-kev range) in decay of Sm^{153}. Shielding of 0.084 cm Pb and 0.122 cm Cd on the crystal feeding the multichannel analyzer and of 0.084 cm Pb, 0.013 cm W, 0.076 gm/cm^2 Ce, and 0.081 cm Cd on the crystal feeding the discriminator was used.

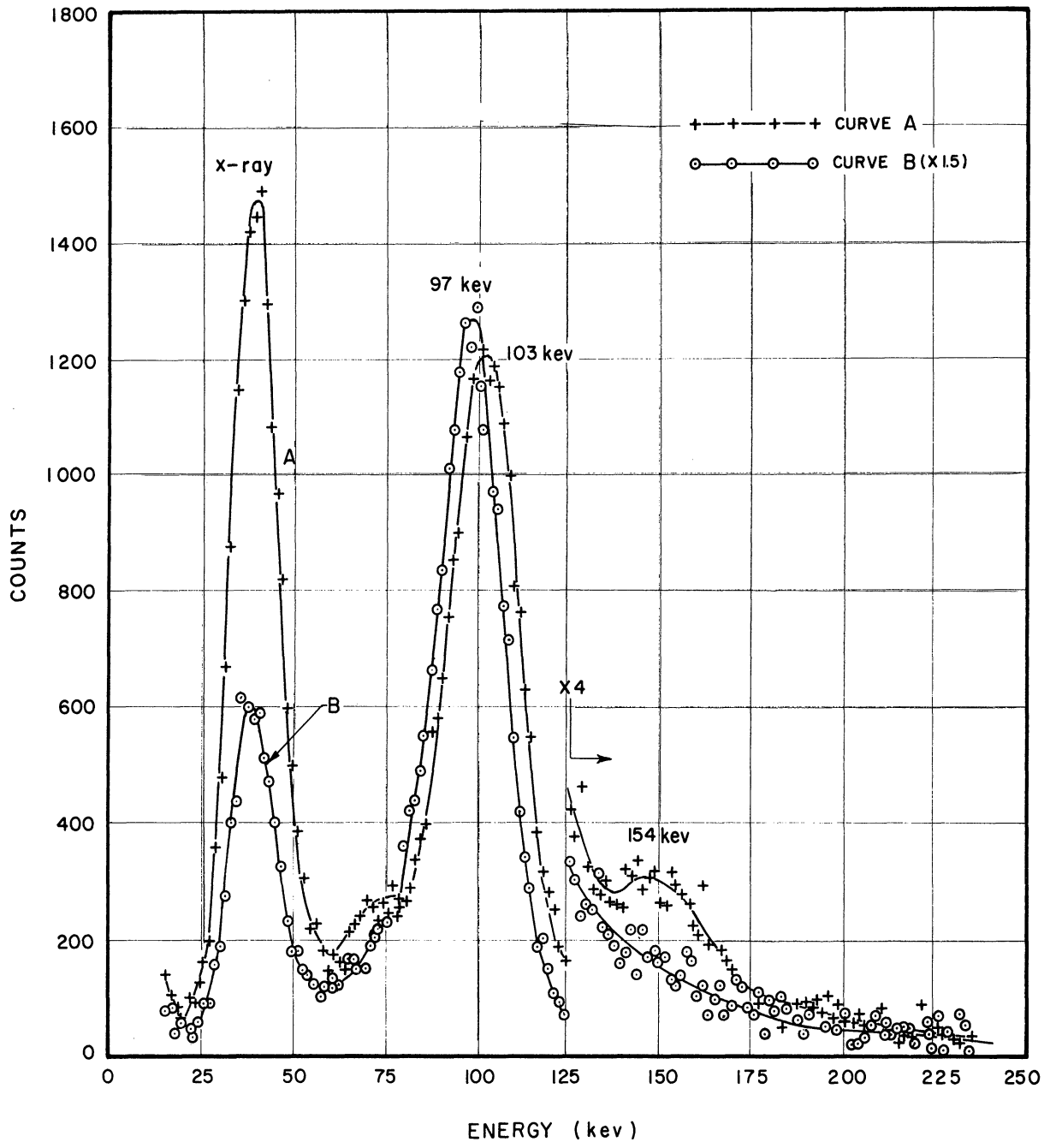

Figure 12. Curve I is the spectrum of coincidences with the 500-kev to 540-kev region in decay of Sm^{153}. Curve II is the spectrum of coincidences with the 612-kev to 665-kev region in decay of Sm^{153}.

The spectrum of gamma rays coincident with the 458-kev transition (445-kev to 475-kev region) is shown in Figure 13. A gamma ray at about 67 kev is shown in addition to the x-ray, 103-kev, and 154-kev transitions. The enhancement of the 67-kev transition and the x-ray is clearly indicated by comparison with the spectrum of coincidences with the 500-kev to 540-kev region.

Figure 14 shows the spectrum of gamma rays in coincidence with the 52-kev to 68-kev range. The 458-kev to 535-kev intensity ratio is considerably enhanced in comparison to the 103-kev coincidence spectrum and to the singles spectrum.

The level structure of Eu^{153} is shown in Figure 15. The levels at 83 kev, 97 kev, 103 kev, 173 kev, and 191 kev, and the corresponding gamma transitions agree with previous results. The level at 638 kev is based on the 535-kev gamma ray coincidence with the 103-kev transition; similarly, the 707-kev level is confirmed by the coincidence between the 97-kev and 610-kev transitions. The 352-kev and 422-kev coincidences with the 173-kev transition support the levels at 525 kev and 595 kev respectively. The proposed 525-kev transition to the ground state agrees with the previously discussed conclusion of another transition near the energy of the 535-kev gamma ray.

The spectrum of coincidences with the 173-kev transition shows that the 458-kev gamma ray is not in coincidence with the 173-kev gamma ray, and therefore is not in coincidence with the 70-kev transition. Similarly, the spectrum of coincidences with the 103-kev transition shows that the 458-kev and 103-kev transitions are not in coincidence.

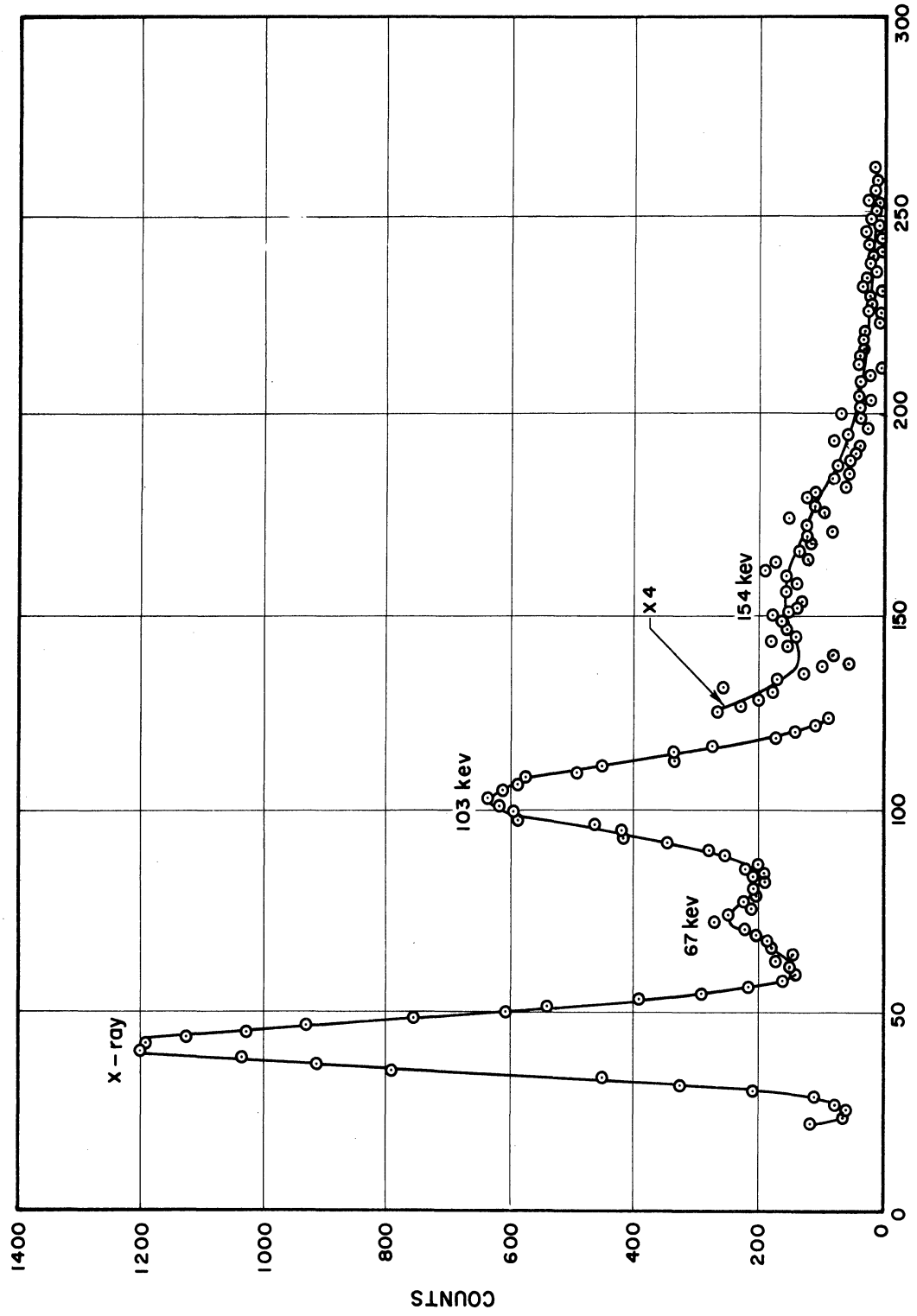

Figure 13. Spectrum of Gamma Rays in Coincidence with the 445-kev to 475-kev Region in Decay of Sm^{153}.

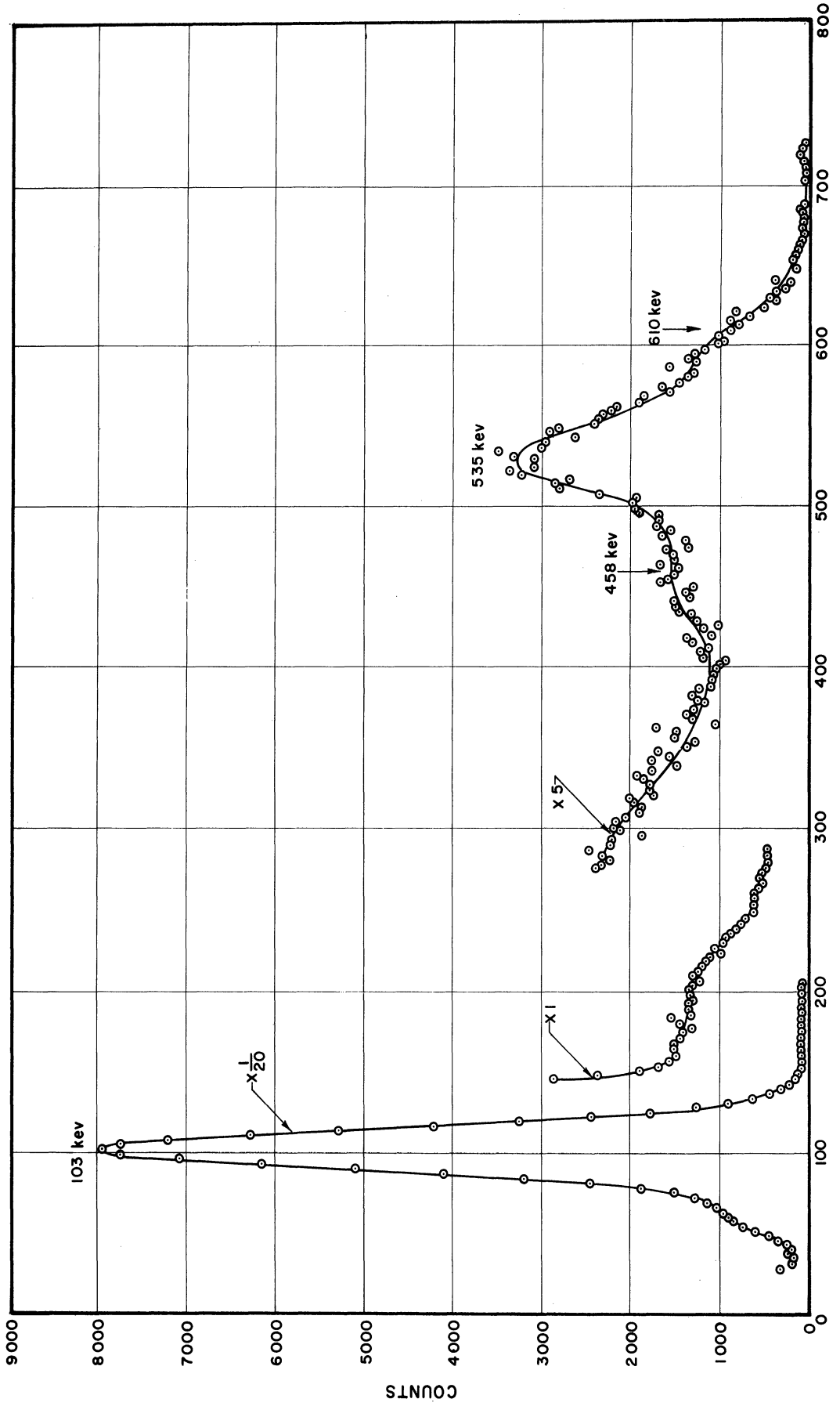

Figure 14. Spectrum of gamma rays in coincidence with the 52-kev to 68-kev range in decay of Sm^{153}. A 0.122 cm Cd absorber was used in front of the crystal feeding the multi-channel analyzer; 0.076 gm/cm^2 of Ce was used in front of the crystal feeding the discriminator.

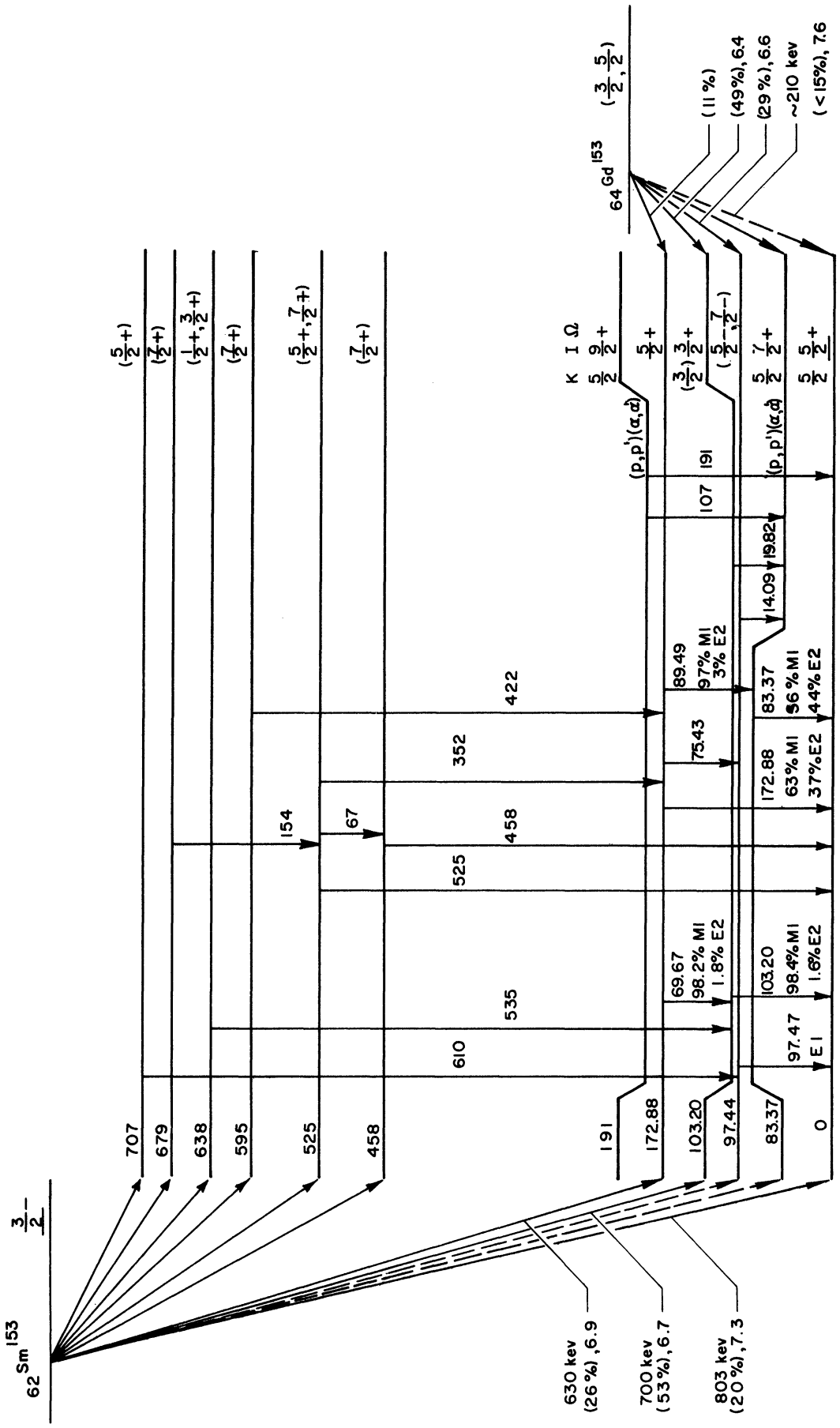

Figure 15. Sm^{153} and Gd^{153} Decay Schemes. The energies are in kev. The numbers after the intensities are log ft values.

The 103-kev gamma ray observed in coincidence with the 445-kev to 475-kev region is from coincidences with the Compton of the 535-kev gamma ray. Since the only gamma rays in coincidence with the 458-kev gamma ray are weak transitions at 67 kev and possibly at 154 kev, the 458-kev transition feeds the ground state. The energy sum of 458 kev and 67 kev agrees with the proposed level at 525 kev. The slight enhancement near 70 kev on the spectrum showing coincidences with the 500-kev to 540-kev region can be attributed to coincidences with the tail of the 458-kev gamma ray.

The spectrum of coincidences with the 52-kev to 68-kev region support the conclusion that the 458-kev gamma ray is in coincidence with the 67-kev gamma ray. The other peaks on this spectrum are mainly due to coincidences with the 70-kev gamma ray and with the iodine x-ray escape peak of the 103-kev transition.

The position of the 154-kev transition in the decay scheme is supported by the coincidence with the 173-kev transition, 458-kev transition, 525-kev transition, and possibly with the 67-kev transition. It is very unlikely that the 154-kev transition feeds the 638-kev level and the corresponding 535-kev transition, since a level would then exist at 792 kev. Only 803 kev are available between the ground states of Sm^{153} and Eu^{153}. Thus the coincidences between the 154-kev gamma ray and the 500-kev to 540-kev region support the existence of a 525-kev gamma ray. The small number of counts at 525-kev on the spectrum of coincidences with the 173-kev transition (166-kev to 191-kev region) are due to coincidences with the tail of the 154-kev gamma ray.

Very weak transitions of 14 kev, 19.8 kev, 75 kev, and 89 kev have been observed in conversion electron spectra of Gd^{153} by Graham et al.[75] Since the levels which feed these gamma rays are excited in the decay of both Gd^{153} and Sm^{153}, these weak transitions also occur in the decay of Sm^{153}. Joshi et al.[61] and Marty[57,58] state that the 83-kev level is possibly weakly excited in the decay of Sm^{153}.

The energies of the levels below 173 kev and of the corresponding transitions shown in Figure 15 are from the internal conversion data on Gd^{153} by Graham et al.[75] Similarly, the multipolarities shown were determined by Graham et al.[75] from experimental L subshell ratios.

The value of α_K for the 70-kev transition was calculated from the x-ray and 70-kev intensities on the spectra of coincidences with the 103-kev transition. Corrections were made for absorption, crystal efficiency, iodine x-ray escape, and x-ray fluorescence yield. A value of 4.4 ± 0.3 was determined.

Using the α_K value for the 70-kev transition and the singles spectrum, the value of α_K for the 103-kev transition was calculated to be 1.14 ± 0.11. This is a mean for calculations from two spectra at source to crystal distances of 2.54 cm and 10.2 cm. The weak transitions have a negligible effect on these calculations.

The value of α_K for the 103-kev gamma ray was also determined from the x-ray and 103-kev intensities on the spectra of coincidences with the 535-kev transition. The resulting α_K is 1.18 ± 0.09. The value of α_K for the 103-kev transition determined from the above two methods is 1.16 ± 0.08.

The α_K for the 97-kev gamma ray can be similarity calculated from the spectra of coincidence with the 610-kev transition (612-kev to 665-kev range). In addition to the previously mentioned corrections, the presence of the tail of the 535-kev transition in the 612-kev to 665-kev range was taken into consideration. The calculated value for α_K is $0.36 \pm \begin{matrix} 0.03 \\ 0.07 \end{matrix}$.

The data of various investigators on values of α_K for the 70-kev, 97-kev, and 103-kev transitions are shown in Table I. The α_K measurements listed in the table for the 103-kev transition in the Gd^{153} decay were computed assuming that there is no 97-kev gamma ray. Since both the 97-kev and 103-kev transitions are strong in the Gd^{153} decay, the measurements fall between the actual values of α_K for the 97-kev and 103-kev transitions. No previous direct determination has been made for α_K in the 97-kev transition. However, the present value of $0.36 \pm \begin{matrix} 0.03 \\ 0.07 \end{matrix}$ agrees with the previous calculations made from α_K for the 103-kev gamma ray and from the relative intensities of the 97-kev and 103-kev conversion electrons and gamma rays in the Gd^{153} decay.

Table II gives the theoretical K-shell internal conversion coefficients from the tables of Sliv and Band[50] for the 70-kev, 97-kev, and 103-kev transitions. The experimental $\alpha_K = 0.36 \pm \begin{matrix} 0.03 \\ 0.07 \end{matrix}$ for the 97-kev gamma ray shows that this transition is predominantly E1. Measurements of the K/L ratio[73,75] and of the L subshell ratios[75] are less conclusive, but are in agreement with this result.

Graham et al.[75] have used L subshell ratios to determine that the 70-kev gamma ray is 98.2% M1 + 1.8% E2 and that the 103-kev gamma ray

TABLE I

MEASURED VALUES OF α_K FOR 70-kev, 97-kev, AND 103-kev TRANSITIONS IN Eu^{153}

Author and Year	Transitions 70 kev	97 kev	103 kev	Isotope Used	Reference
Siegbahn, 1952			0.65	Sm^{153}	53
Graham and Walker, 1954	5.7 ± 1.0			Sm^{153}	54
Lee and Katz, 1954			0.62 ± 0.15	Sm^{153}	55
McGowan, 1954	3.8 ± 0.2		1.14 ± 0.20	Sm^{153}	56
Marty, 1955			1.2 ± 0.1	Sm^{153}	58
Dubey et al., 1956	4.4 ± 0.4		1.19 ± 0.15	Sm^{153}	60
Joshi et al., 1957	3.5 ± 1.4		0.69 ± 0.08	Sm^{153}	61
Cohen et al., 1955			1.2	Gd^{153}	67
Bhattacherjee and Raman, 1956			0.67 ± 0.12	Gd^{153}	68
Bisi et al., 1956			0.70 ± 0.03	Gd^{153}	69
Gupta and Jha, 1956			0.61 ± 0.03	Gd^{153}	70
Marty and Vergnes, 1956		0.3 ± 0.1		Gd^{153}	71
Joshi and Subba Rao, 1957		0.15± 0.04*		Gd^{153}	72
McCutchen, 1958		<0.4		Gd^{153}	51
present measurement	4.4 ± 0.3	$0.36^{+0.03}_{-0.07}$	1.16 ± 0.08	Sm^{153}	

* based on $\alpha_{K\text{-}103} = 0.69$

is 98.4% M1 + 1.6% E2. The experimental values of K/L ratios[73,75] and of α_K agree with these assignments.

The total internal conversion coefficients for the 70-kev, 97-kev, and 103-kev transitions were calculated to be 5.1 ± 0.5, $0.41 \begin{smallmatrix} + 0.04 \\ - 0.08 \end{smallmatrix}$, and 1.38 ± 0.11 respectively. The contributions from the L conversion coefficients were obtained from the data of Sliv and Band.[50]

The relative intensities of the gamma rays from the decay of Sm^{153} are shown in Table III. The intensities of the gamma rays at 70 kev, 103 kev, 173 kev, 422 kev, 458 kev, 525 kev plus 535 kev, and 610 kev were computed from the singles spectra. Corrections were made for crystal efficiency and photofraction, iodine x-ray escape, and absorption. The 352-kev gamma ray intensity was determined from its relative intensity to the 422-kev transition on the spectrum of coincidences with the 173-kev gamma ray.

The 67-kev gamma ray intensity was calculated from the ratio of the 67-kev and 103-kev intensities on the spectrum of coincidences with the 445-kev to 475-kev region. Use was made of the fact that the 535-kev transition feeds the 103-kev level and that about 40% of the total counts in the 445-kev to 475-kev region are due to the Compton of the 535-kev gamma ray. In a similar manner the 154-kev gamma ray intensity was calculated from the spectra of coincidences with the 525-kev transition (500-kev to 540-kev region). A small correction was made to the 154-kev gamma ray intensity to account for the de-excitation of the 525-kev level by the 352-kev and 67-kev transitions, in addition to the 525-kev transition. Because of the branching ratios, much of the 154-kev gamma ray observed

TABLE II

K-SHELL INTERNAL CONVERSION COEFFICIENTS
FOR 70-kev, 97-kev, AND 103-kev TRANSITIONS IN Eu^{153}

Gamma-Ray	Experimental	Theoretical Values[50]			
Energy	Value	E1	E2	M1	M2
70 kev	4.4 ± 0.3	0.63	2.8	4.4	51.
97 kev	$0.36 \begin{smallmatrix} +0.03 \\ -0.07 \end{smallmatrix}$	0.26	1.2	1.7	15.
103 kev	1.16 ± 0.08	0.23	1.1	1.4	12.

- - - - - - -

TABLE III

RELATIVE INTENSITIES OF THE GAMMA TRANSITIONS FROM DECAY OF Sm^{153}

(The intensities have been normalized to the 103-kev transition. The errors on the intensities for the 67-kev, 154-kev, 173-kev, 352-kev, and 422-kev gamma rays are large.)

E_γ(kev)	Gamma-Ray Intensity	α	Transition Intensity
67	0.07		
70	130 ± 20	5.1 ± 0.5	330 ± 50
97	< 50		
103	1000	1.38 ± 0.11	1000
154	0.07		
173	1.8	0.35	1.0
352	0.24		
422	0.16		
458	0.5 ± 0.2		
525	1.3 ± 0.5		
535	3.5 ± 0.5		
610	1.1 ± 0.4		

on the spectra of coincidences with the 166-kev to 191-kev region can be attributed to coincidences with the Compton of the 525-kev transition.

The intensity limit for the 97-kev gamma ray shown in Table III is from the measurements with a bent-crystal spectrometer by Walters et al.[65]

The 83.4-kev gamma ray is less than 4% of the 103-kev gamma ray intensity in the Sm^{153} decay.[57,58,61] The transitions[75] at 14 kev, 19.8 kev, 75 kev, 83.4 kev, and 89 kev were not within the limits of observation of the present research and are therefore not included in the table.

In computing the transition intensity for the 173-kev transition, the theoretical value of α was determined from the tables of Sliv and Band,[50] using a multiple mixture[75] of 63% M1 + 37% E2.

The beta transition feeding the ground state has an intensity of 20% and an energy of 803 kev.[54,55,58,60,61,63] The intensities and energies of the reamining beta transitions have been determined from the gamma ray intensities and energies. The log ft values have been computed using these values.

Directional Correlation Measurements

The directional correlation for the 70-kev — 103-kev cascade was measured by accepting pulses in the energy range from 70-kev to 115-kev in both differential analyzers. After correcting for finite resolution,[47] the expansion coefficients from the measurements of the Sm^{153} decay were found to be $A_2 = 0.005 \pm 0.007$ and $A_4 = -0.007 \pm 0.011$. The results for the Gd^{153} decay are $A_2 = 0.006 \pm 0.010$ and $A_4 = -0.007 \pm 0.016$. Very dilute solutions were used in making both measurements.

The ground state spin[79,80] of Eu^{153} has been measured to be 5/2. The deformation parameter of 0.30 results in an assignment[16] to Nilsson orbit 27, which has a spin of 5/2+. The spin[81] of Sm^{153} has been determined as 3/2. This is presumably the Nilsson[16] orbit 52, which is the expected ground state for N = 91 near a deformation of 0.25. Alaga[17] has used selection rules for large nuclear deformation in analyzing the beta transition between the Sm^{153} and Eu^{153} ground states. The log ft value of 7.3 indicates that the transition is hindered first forbidden. This is in agreement with the spin and parity assignments.

The 83-kev and 191-kev levels observed in Coulomb excitation have been assigned spins[76-78] of 7/2+ and 9/2+, respectively, on the basis of the gamma ray multipolarities and the weakness of the beta transitions feedings these levels from Sm^{153}.

The M1 + E2 nature[75] of the 103-kev gamma ray indicates that the spin of the 103-kev level is 3/2+, 5/2+, or 7/2+. Since the beta transition feeding the 103-kev level is first forbidden, the spin is further limited to 3/2+ or 5/2+.

The M1 + E2 multipolarity[75] of the 70-kev, 89-kev, and 173-kev gamma rays allows spins of 5/2+ or 7/2+ for the 173-kev level. The log ft value of 6.9 for the beta transition feeding the 173-kev level indicates that the spin of this level is 5/2+.

In interpreting the angular correlation data, the multipolarities[75] of 98.2% M1 + 1.8% E2 for the 70-kev gamma ray and 98.4% M1 + 1.6% E2 for the 103-kev transition were used. A reasonable error limit of $\pm$ 1% for the quadrupole contents of both gamma rays was used

in making the analysis. The A_2 versus Q (quadrupole content) curve for a spin 3/2 intermediate state and spin 5/2 ground state has a value of zero at Q = 0.008. Therefore, the experimental $A_2 = 0.005 \pm 0.007$ for the cascade agrees with the spin assignments of 3/2 and 5/2 for the 103-kev level and ground state respectively. In this case, the angular correlation does not limit the spin of the 173-kev level. Therefore the previously concluded value of 5/2+ for this level is allowed.

One spin sequence which is consistent with previous experimental data, but unlikely, is (5/2+, 5/2+, 5/2+) for the 173-kev, 103-kev, and ground state levels. The sequence is ruled out by the angular correlation results.

Therefore, the only sequence allowed by experimental data for the levels at 173-kev, 103-kev, and the ground state is (5/2+, 3/2+, 5/2+).

Since the 97-kev gamma ray is E1, possible spins for the 97-kev level are 3/2-, 5/2-, or 7/2-. The weakness of the 97-kev gamma ray from the Sm^{153} decay and the strong intensities of the 97-kev and 103-kev transitions from the Gd^{153} decay indicate that the 97-kev level has spin 7/2- or possibly 5/2-.

The beta transitions feeding the high energy levels have log ft values which are first forbidden and first forbidden unique. This information and the relative gamma ray intensities suggest the spin assignments shown in Figure 15 for the high energy states.

Lee and Katz[55] observed an internal conversion line for the 535-kev transition. A re-interpretation of their data for α_K results in a high order of multipolarity (M3, M4, E4) for the 535-kev transition.[51,58]

However, Marty[58] was not able to observe any internal conversion electrons for the 535-kev transition in the presence of the beta rays. The magnitude of the internal conversion coefficient should be rechecked.

Results for Gd^{153} Decay

Gamma-Ray Spectra

Figure 16 I shows the gamma ray spectrum from the Gd^{153} decay. This spectrum was taken at the same time and with the same geometry and absorbers as the Se^{81m} and Sm^{153} spectra shown in Figure 8. A comparison of Gd^{153} and Sm^{153} spectra indicates the presence of a strong 97-kev gamma ray in the Gd^{153} decay, in addition to the 103-kev gamma ray and a weak 70-kev gamma ray. The peak at 142-kev in the Gd^{153} spectrum is due to the x-ray summing with the gamma rays in the 100-kev region.

Curve II of Figure 16 is the Se^{81m} spectrum with the energy axis shifted so that the peaks in the 100-kev region correspond in the Se^{81m} and Gd^{153} spectra. The very weak Compton distribution from high energy transitions was subtracted to obtain the Se^{81m} spectrum shown. After making corrections for absorption, crystal efficiency, and iodine x-ray escape, the relative intensity of the 70-kev gamma ray to the 97-kev and 103-kev gamma rays was calculated to be 0.04 ± 0.02 for a source to crystal distance of 2.54 cm. The same result was obtained for a source to crystal distance of 10.2 cm.

Figure 17 shows the gamma ray spectrum taken with a strong source and suitable absorbers. From Figure 17 and Figure 7B the ratio of the 173-kev gamma ray to the gamma rays in the 100-kev region in the Gd^{153} decay compared to the same ratio in the Sm^{153} decay is 0.37 ± 0.18.

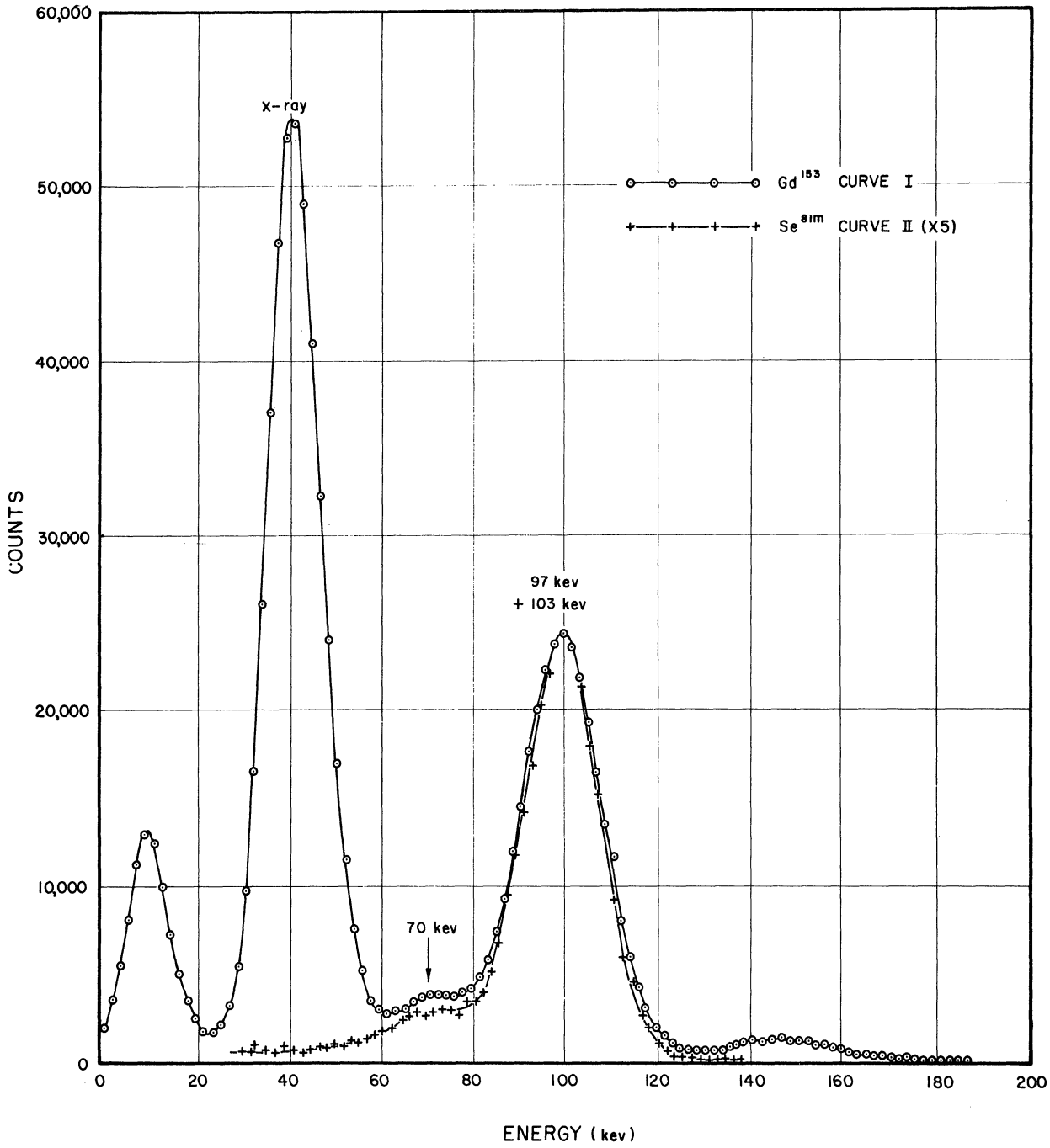

Figure 16. Curve I is scintillation spectrum of gamma rays in decay of Gd^{153}. The peak at 12 kev is due to the iodine x-ray escape for the Eu x-ray. Curve II is the scintillation spectrum of gamma rays from decay of Se^{81m}. The energy axis in curve II is shifted so that the peaks in the region of 100 kev in the Sm^{153} and Gd^{153} spectra correspond. Both spectra were taken at a source to crystal distance of 2.54 cm.

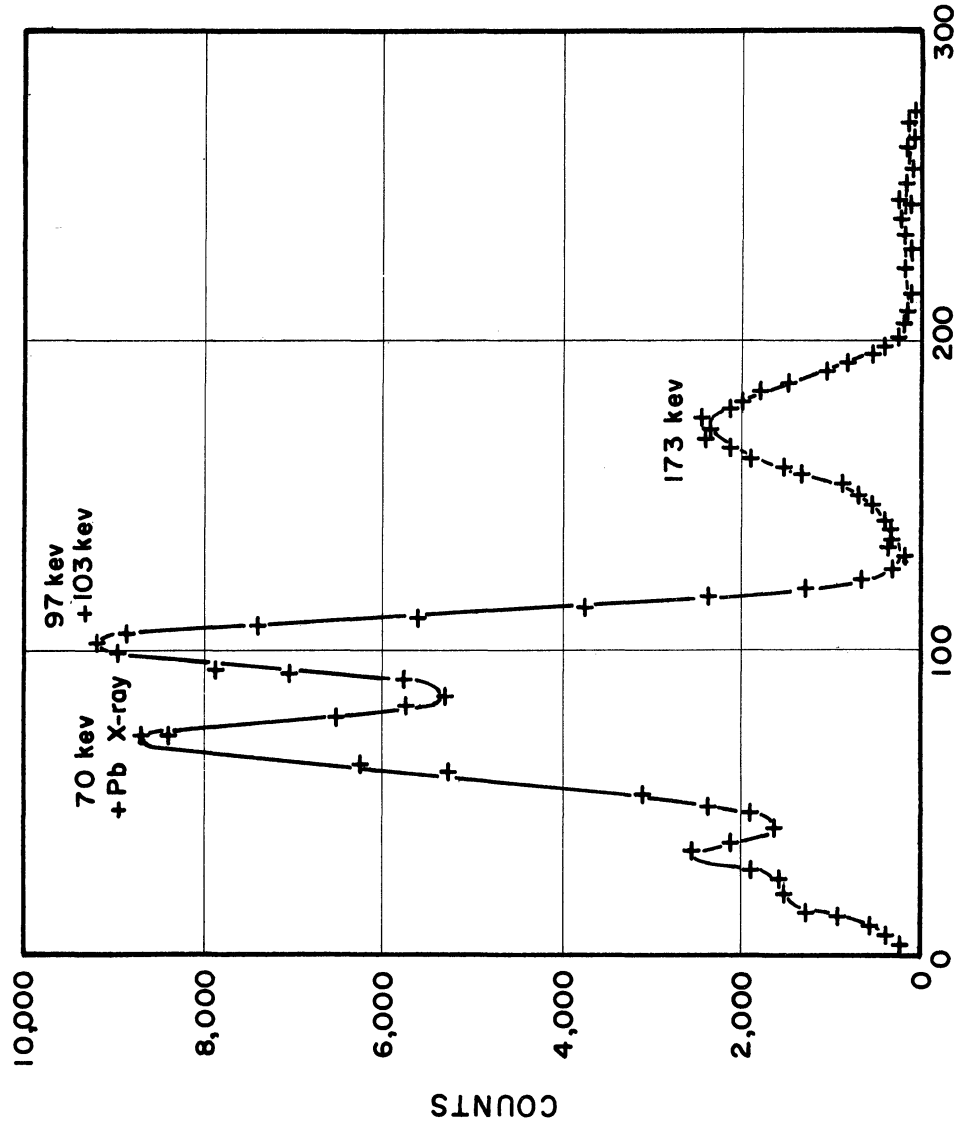

Figure 17. Scintillation spectrum of gamma rays in decay of Gd^{153}. The spectrum was taken with the Gd^{153} source at 5.7 cm from the crystal and with absorbers of 0.084 cm Pb, 0.013 cm W, and 0.203 cm Cd. A small contribution from Eu^{152} and Tb^{160} impurities was subtracted to obtain the spectrum.

This agrees with 0.32 ± 0.18, which is the corresponding ratio for the 70-kev gamma ray and the gamma rays in the 100-kev region.

Coincidence Measurements

The spectrum of gamma rays in coincidence with the 97-kev and 103-kev transitions (90-kev to 111-kev range) is shown in Figure 18. Peaks are shown at the x-ray and at 70 kev. The x-ray coincidence is mainly from the K-capture x-ray preceding the 97-kev and 103-kev transitions. The small peak at 103 kev is due to coincidences with the tail of the 70-kev transition.

Figure 19A illustrates the spectra of gamma rays in coincidence with the x-ray (36-kev to 46-kev range) in the decay of Sm^{153} and Gd^{153}. Peaks are shown at the x-ray, 70 kev, and 103 kev for the Sm^{153} decay, and at the x-ray, 70 kev, 97 kev, and 103 kev for the Gd^{153} decay.

The spectra of gamma rays coincident with the 70-kev transition (70-kev to 80-kev range) in the decay of Sm^{153} and Gd^{153} are shown in Figure 19B. Peaks are shown at the x-ray, 70 kev, and 103 kev in both cases. The peaks at 70 kev are due to coincidences with the iodine x-ray escape peak of the 103-kev transition. The large x-ray intensity on the Gd^{153} spectrum is mainly due to K-capture x-ray coincidences with the escape peaks of the 97-kev and 103-kev gamma rays.

The coincidence measurements on the Gd^{153} decay agree with the previous results[51,75] for the level structure in Eu^{153}, as shown in Figure 15.

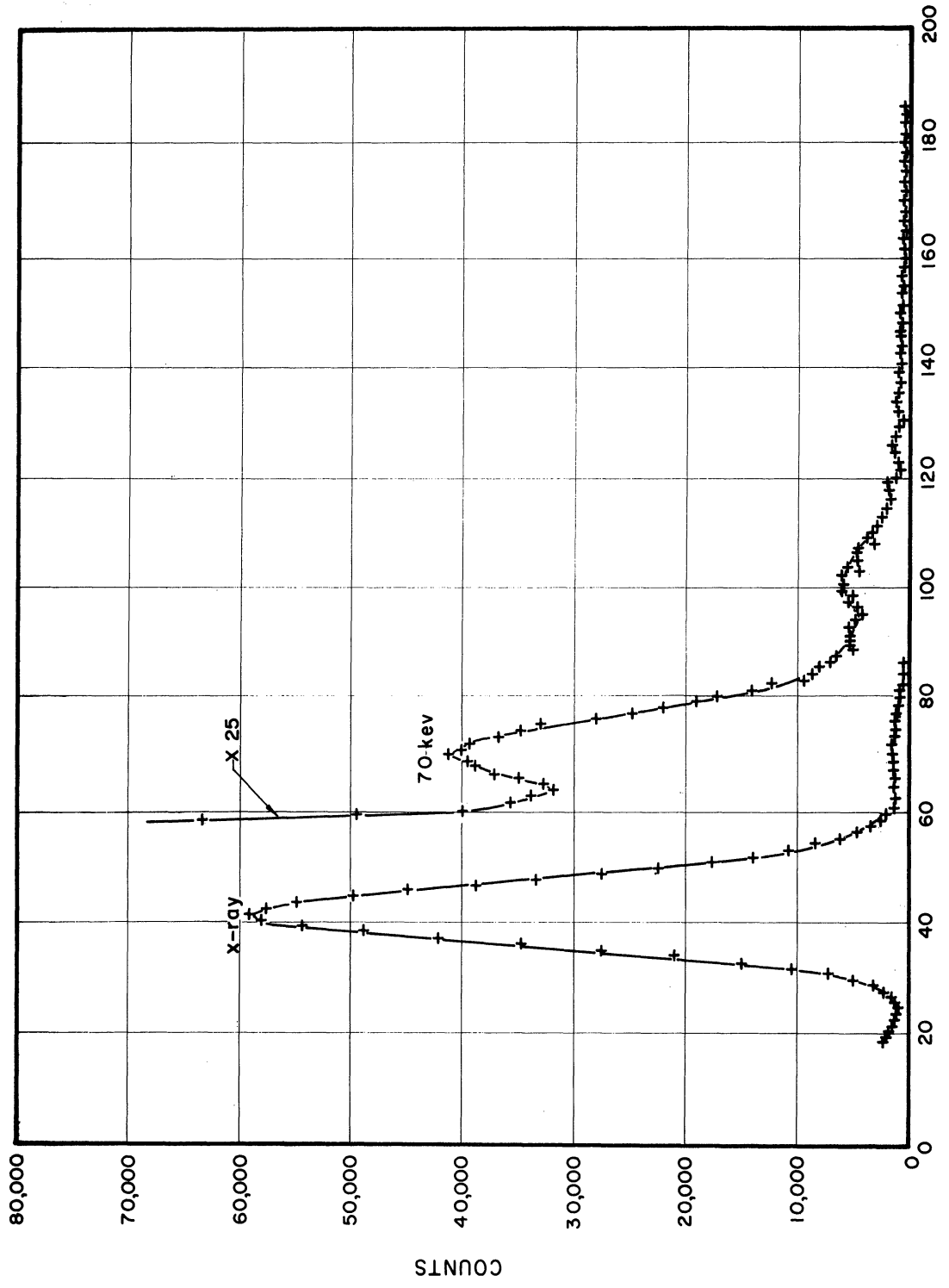

Figure 18. Spectrum of Gamma Rays in Coincidence with 90-kev to 111-kev Region in Decay of Gd^{153}.

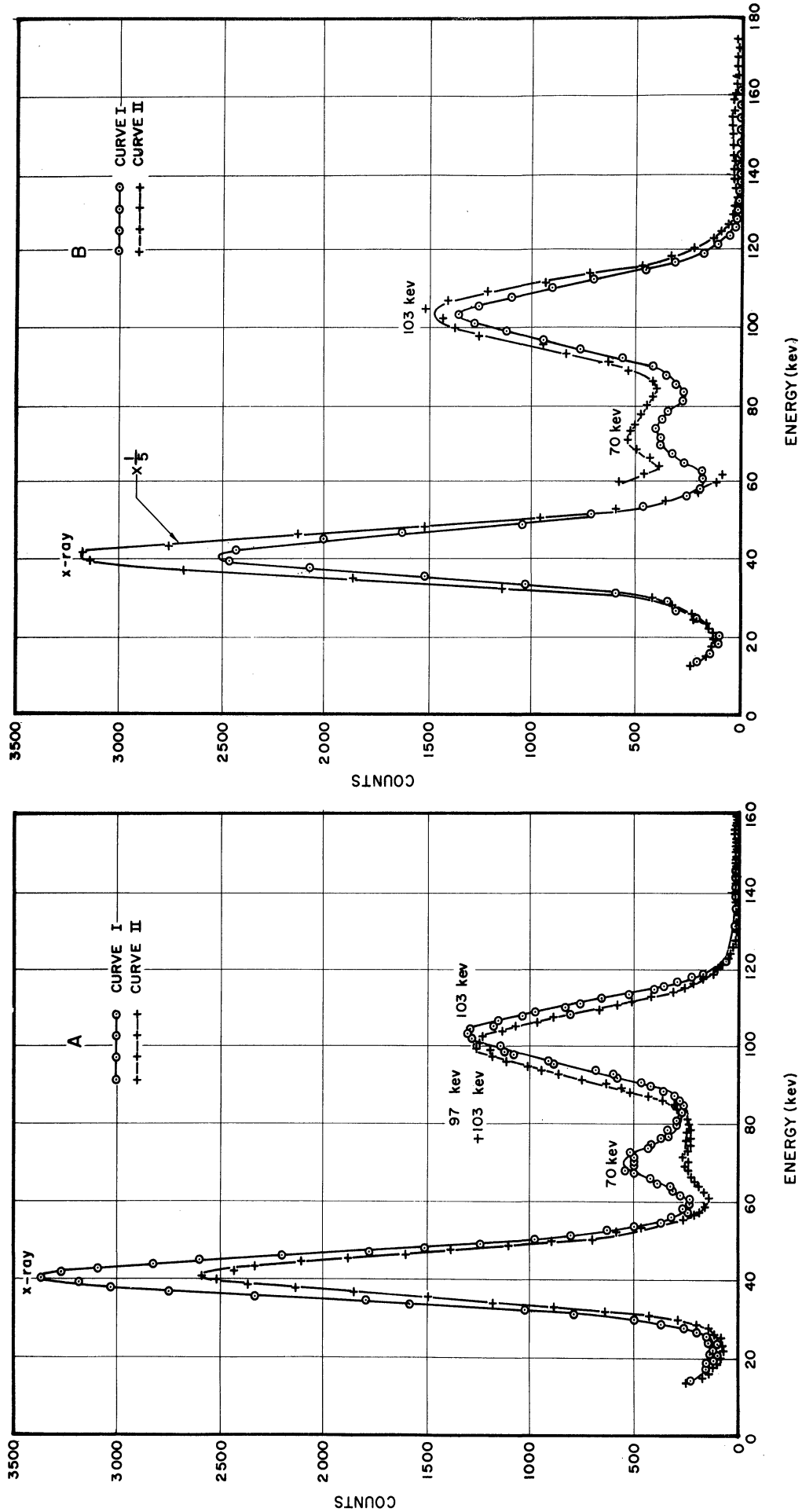

Figure 19. The spectra of coincidences with the 36-kev to 46-kev region in the decay of Sm^{153} and Gd^{153} are shown in curves AI and AII respectively. The spectra of coincidences with the 70-kev to 80-kev region in the decay of Sm^{153} and of Gd^{153} are shown in curves BI and BII respectively.

The 97-kev to 103-kev gamma ray intensity ratio was computed from the K-shell internal conversion coefficients and the intensities of the K-shell internal conversion electrons of these transitions. Graham et al.[75] found the ratio of the K-shell electrons for the 97-kev and 103-kev transitions to be 0.253. The ratio of the 97-kev to 103-kev gamma ray intensities computed in this way is $0.81 \begin{smallmatrix} + 0.17 \\ - 0.09 \end{smallmatrix}$. A comparison with previously determined ratios is shown in Table IV. In these determinations the 97-kev and 103-kev gamma rays are weakly resolved in both the external conversion[72] and xenon counter[51] spectra. These two spectra[51,72] each had approximately 135 counts at their maxima.

The relative intensities of the gamma rays from the decay of Gd^{153} are shown in Table V. The ratio of the 70-kev gamma ray to 97-kev and 103-kev gamma rays was computed from the singles spectra. The 173-kev intensity was determined from the 70-kev intensity in Gd^{153} decay and the 173-kev to 70-kev gamma ray intensity ratio in Sm^{153} decay.

The 14-kev, 19.8-kev, 75.4-kev and 89.5-kev transitions have intensities which range from about 0.2% to 0.7% of the 103-kev transition intensity, and the intensity of the 83-kev transition is about 1.7% of the 103-kev transition intensity.[75] These gamma rays are not included in the table, since they were not within the limits of observation of the present research.

The decay energy between Gd^{153} and Eu^{153} has been calculated by several investigators from the experimental ratio of L to K capture. The various values obtained for the total disintegration energy range from 186 kev to 225 kev.[68-71] Due to the simplified decay schemes

TABLE IV

MEASURED VALUES OF THE INTENSITY RATIO OF 97-kev GAMMA RAY TO THE 103-kev GAMMA RAY IN THE DECAY OF Gd^{153}

Author	Intensity Ratio	Method	Reference
Marty and Vergnes	1.05 ± 0.35	Decomposing scintillation spectrum	71
	0.9 ± 0.2	Intensity ratios in spectra of Sm^{153} and Gd^{153}	71
Joshi and Subba Rao	1 ± 0.1	External conversion spectrum	72
McCutchen	1.74	Xenon counter spectrum	51
Present determination	$0.81 \begin{smallmatrix} +0.17 \\ -0.09 \end{smallmatrix}$	Internal conversion coefficients and electron intensity ratio	

- - - - - - - -

TABLE V

RELATIVE INTENSITIES OF THE GAMMA TRANSITIONS FROM DECAY OF Gd^{153}

(The intensities have been normalized to the 103-kev transition. The errors for the 173-kev transition are large.)

E_γ(kev)	Gamma-Ray Intensity	α	Transition Intensity
70	73 ± 37	5.1 ± 0.5	187 ± 83
97	$810 \begin{smallmatrix} +170 \\ -90 \end{smallmatrix}$	$0.41 \begin{smallmatrix} +0.04 \\ -0.08 \end{smallmatrix}$	$482 \begin{smallmatrix} +83 \\ -54 \end{smallmatrix}$
103	1000	1.38 ± 0.11	1000
173	1.0	0.35	0.6

- - - - - - - -

assumed in these determinations and the nature of the calculations, the errors are expected to be large. Using similar techniques, the values calculated for the intensity of the transition to the ground state of Eu^{153} vary from 0% to 25%.[67-70]

The electron capture intensities and log ft values shown in Figure 15 for the Gd^{153} decay were computed on the basis that the transition to the Eu^{153} ground state has an energy of 210 kev and an intensity of 10%. The gamma ray energies and intensities were used in these determinations.

Discussion

The nuclear deformation[16] changes from 0.16 to 0.30 in going from $^{88}_{63}Eu^{151}$ to $^{90}_{63}Eu^{153}$. Mottelson and Nilsson[15] attribute this change to the existence of two minima in the curve of nuclear energy as a function of deformation. At neutron number N = 88 the energy minimum corresponding to the smaller deformation has a value less than the other energy minimum; at N = 90 the opposite effect takes place. For N = 90 excited intrinsic states corresponding to the minimum at small deformations may exist. Transitions involving a large change in the nuclear shape would be expected to have a reduced transition probability.

Mottelson and Nilsson[15] suggest that in Eu^{153} the ground state, 103-kev level, and 173-kev level correspond to the larger deformation ($\sim$ 0.3) and that the 97-kev level has the smaller deformation. The 3/2+ level at 103 kev may be assigned to Nilsson[16] orbit 33. The state at 97 kev has been assigned a spin of 7/2- or 5/2- on the basis of experimental data. This state possibly corresponds to Nilsson[15,16] orbit

36 with spin 5/2-. The weakness of the beta ray feeding the 97-kev level in the Sm^{153} decay may be due to the large change in nuclear shape in such a transition.(15)

The 83-kev and 191-kev levels are rotational excitations(9) of the ground state with the expected spin values of 7/2+ and 9/2+ respectively.

Several authors(15,74) have suggested that the 173-kev state (5/2+) is a rotational level associated with the 3/2+ 103-kev state in an effort to explain the high intensity of the 70-kev gamma ray relative to the 173-kev gamma ray. However, Graham et al.(75) have shown that the experimental reduced transition probabilities do not agree with the theoretical reduced transition probabilities for rotational states based on the proposed K value of 3/2 for the 103-kev and 173-kev levels.

The ground state spin of Gd^{153} has not been measured. The log ft values for the Gd^{153} decay feeding the 97-kev and 103-kev levels indicate that Gd^{153} has a spin of 3/2 or 5/2. The deformation of Gd^{153} is uncertain, but may be small.(15) Nilsson orbit 57 with a spin of 3/2+ is a possible assignment.(15,16) In this case the log ft value would indicate a spin of 5/2- for the 97-kev state and the transition to this level would be hindered first forbidden, according to the selection rules of Alaga.(15,17) The transitions to the ground state, 103-kev state, and 173-kev state would be hindered allowed.(15) Retardation effects may also exist due to changes in the nuclear deformation.

36 with spin 5/2-. The weakness of the beta ray feeding the 97-kev level in the Sm^{153} decay may be due to the large change in nuclear shape in such a transition.(15)

The 83-kev and 191-kev levels are rotational excitations(9) of the ground state with the expected spin values of 7/2+ and 9/2+ respectively.

Several authors(15,74) have suggested that the 173-kev state (5/2+) is a rotational level associated with the 3/2+ 103-kev state in an effort to explain the high intensity of the 70-kev gamma ray relative to the 173-kev gamma ray. However, Graham et al.(75) have shown that the experimental reduced transition probabilities do not agree with the theoretical reduced transition probabilities for rotational states based on the proposed K value of 3/2 for the 103-kev and 173-kev levels.

The ground state spin of Gd^{153} has not been measured. The log ft values for the Gd^{153} decay feeding the 97-kev and 103-kev levels indicate that Gd^{153} has a spin of 3/2 or 5/2. The deformation of Gd^{153} is uncertain, but may be small.(15) Nilsson orbit 57 with a spin of 3/2+ is a possible assignment.(15,16) In this case the log ft value would indicate a spin of 5/2- for the 97-kev state and the transition to this level would be hindered first forbidden, according to the selection rules of Alaga.(15,17) The transitions to the ground state, 103-kev state, and 173-kev state would be hindered allowed.(15) Retardation effects may also exist due to changes in the nuclear deformation.

CHAPTER VI

THE LEVEL STRUCTURE OF Eu^{155}

Introduction

A 21-minute activity from samarium was first observed by Pool and Quill.[82] Inghram et al.[83] and Winsberg[84] assigned this activity to Sm^{155}. Rutledge et al.[85] observed gamma rays of 104.6 kev and 245.8 kev on internal conversion and photoelectron spectrograms. Schmid and Burson[86] obtained coincidences between the 105-kev gamma ray and a gamma ray of 141 kev, and proposed the decay scheme shown in Figure 20.

Because of the position of Sm^{155} in the region of $150 < A < 190$, it is expected that the excited levels in Eu^{155} will exhibit the characteristics of deformed nuclei. The present investigation was undertaken in order to study more completely the excited levels occurring in Eu^{155}.

Experimental Method

Samples of samarium oxide enriched to 99.1% in Sm^{154} were irradiated in a flux of 2×10^{12} neutrons/cm^2/sec in the Ford Nuclear Reactor. Except for half-life measurements, all data were taken during the first 30 minutes after irradiation.

The radiation time for the magnetic spectrometer sources averaged about 20 minutes, and the exposure time was about 25 minutes. The elapsed time between removing the sources from the reactor and starting the exposure on the photographic plate was about 3 minutes. Three spectrograms of 23, 25, and 59 exposures were taken. When the Sm^{155} had decayed sufficiently after each spectrogram, a photographic plate was exposed

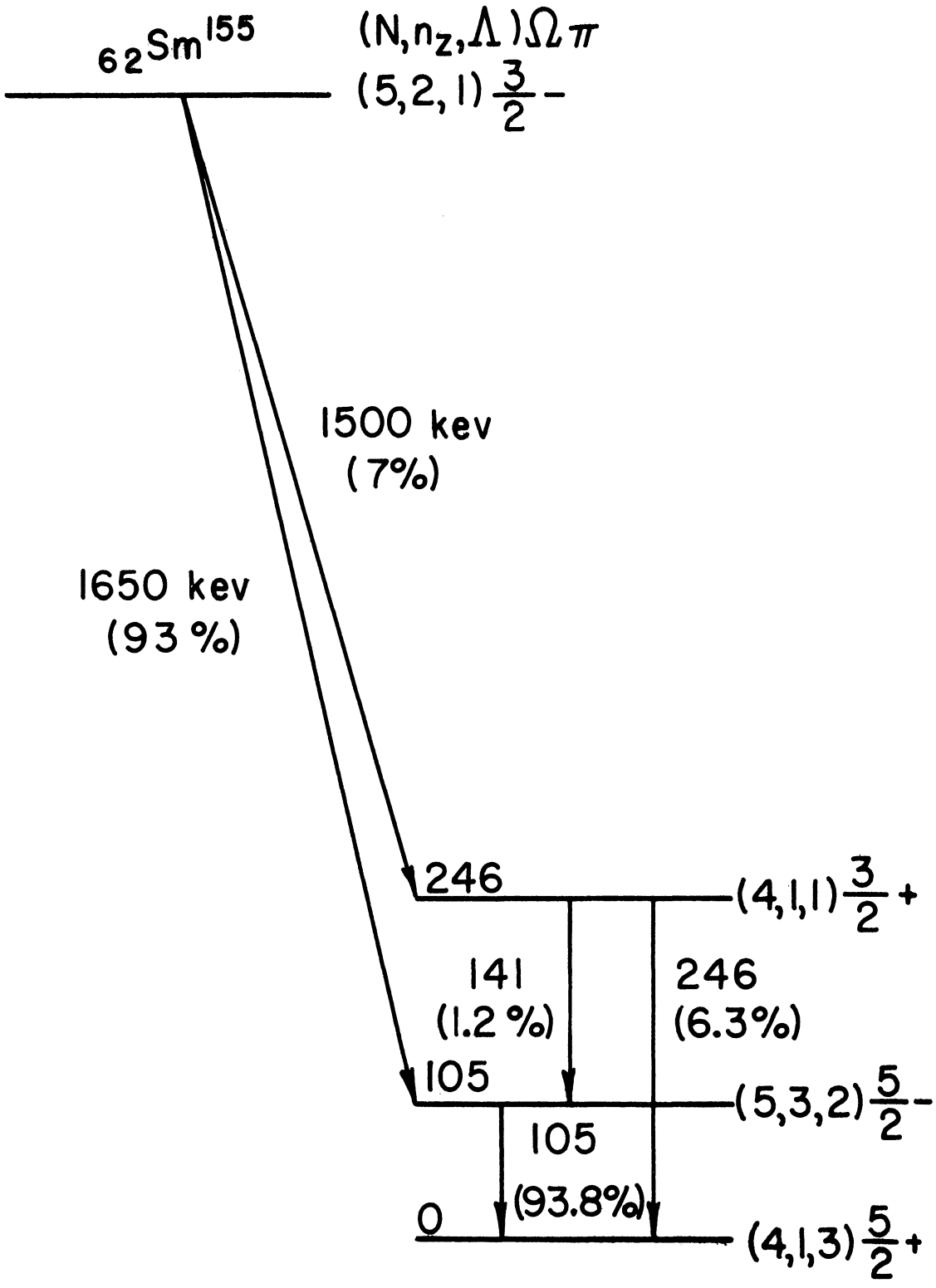

Figure 20. Decay Scheme of Sm^{155}, Due to Schmid and Burson.[86]

for a long time with one of the samples to determine which lines were due to the 47-hour Sm^{153}. Sources of Eu^{152m} and Dy^{165} were used to calibrate the plates.

The sources used in the half-life determination, gamma ray spectra, coincidence measurements, and the directional correlation measurements were made by dissolving the Sm_2O_3 powder in dilute nitric acid and irradiating the samples from 10 seconds to 3 minutes.

Results and Discussion

Half-Life Measurement

The half-life of Sm^{155} was followed for 31 hours, and the 47-hour Sm^{153} activity did not become significant until after approximately eight half-lives had elapsed. The counting rates were corrected for background, the Sm^{153} activity, and Geiger tube dead time. A least squares fit was made on two sets of data, and a value of 21.9 ± 0.2 minutes was determined for the half-life. The error includes the probable error and also an estimate of the systematic error.

Magnetic Spectrograph Measurements

Twelve conversion electron lines corresponding to nine gamma-ray transitions were observed in the spectrograph measurements. The conversion electron energies for Sm^{155} and their assignments are given in Table VI. The line with electron energy of 57.2 kev was on the order of a hundred times weaker than the K line of the 104-kev transition and could possibly be explained by external conversion of the 104-kev transition in Sm. This weak line together with internal conversion lines

TABLE VI

MAGNETIC SPECTROGRAPH MEASUREMENTS FOR Sm^{155}

Electron Energy (kev)	Assignment		(kev)	Strength[a]
29.7		K	78.2	w
	or	L	37.	
33.3		K	81.8	w
	or	L	41.	
55.8		K	104.3	vvs
57.2		K(Eu)	105.7	w
	or	K(Sm)[b]	104.3	
	or	L(Eu)	65.0	
65.2		K	113.7	w
71.1		K	119.6	m
77.0		K	125.5	w
93.4		K	141.9	m
96.8		L	104.3	vs
103.0		M	104.3	s
104.9		K	153.4	w
197.		K	246.	m

[a] v = very, s = strong, m = medium, w = weak

[b] Possibly photoelectrons from Sm

from the 104-kev and 246-kev transitions has been observed previously.[85] A spectrogram of blank Scotch tape sources taken under conditions similar to the samarium sources showed no lines.

Well-Crystal Spectra

Figure 21 shows the gamma ray spectrum as recorded on a 256-channel analyzer. Figure 22 is a spectrum taken with a weak source in a 2-in. x 2-in. NaI(Tl) well crystal. The well-crystal spectrum shows an enhancement of the 246-kev gamma ray, corresponding to a sum of the 104-kev and 142-kev transitions. There is also a peak at 288 kev from the 246-kev gamma ray summing with the x-ray.

The peak at about 75 kev in the spectrum could be caused by the iodine x-ray from the 104-kev gamma ray escaping from the crystal. The ratio of the 75-kev peak to the 104-kev peak was 6% in the "singles" spectrum and 3% in the well-crystal spectrum. The theoretical value for the relative intensity of the iodine x-ray escape peak to the total peak for gamma rays entering perpendicular to an infinite NaI surface is about 4% for a 104-kev gamma ray.[87] The experimental ratios for a source distance of 0.4 cm are somewhat larger than the calculated values.[87]

Coincidence Measurements

Figure 23 illustrates the spectrum of lines in coincidence with the x-ray. In addition to coincidences with the x-ray, 104-kev gamma ray, and 142-kev gamma ray, coincidences are shown with a gamma ray of about 68 kev and with the 246-kev transition.

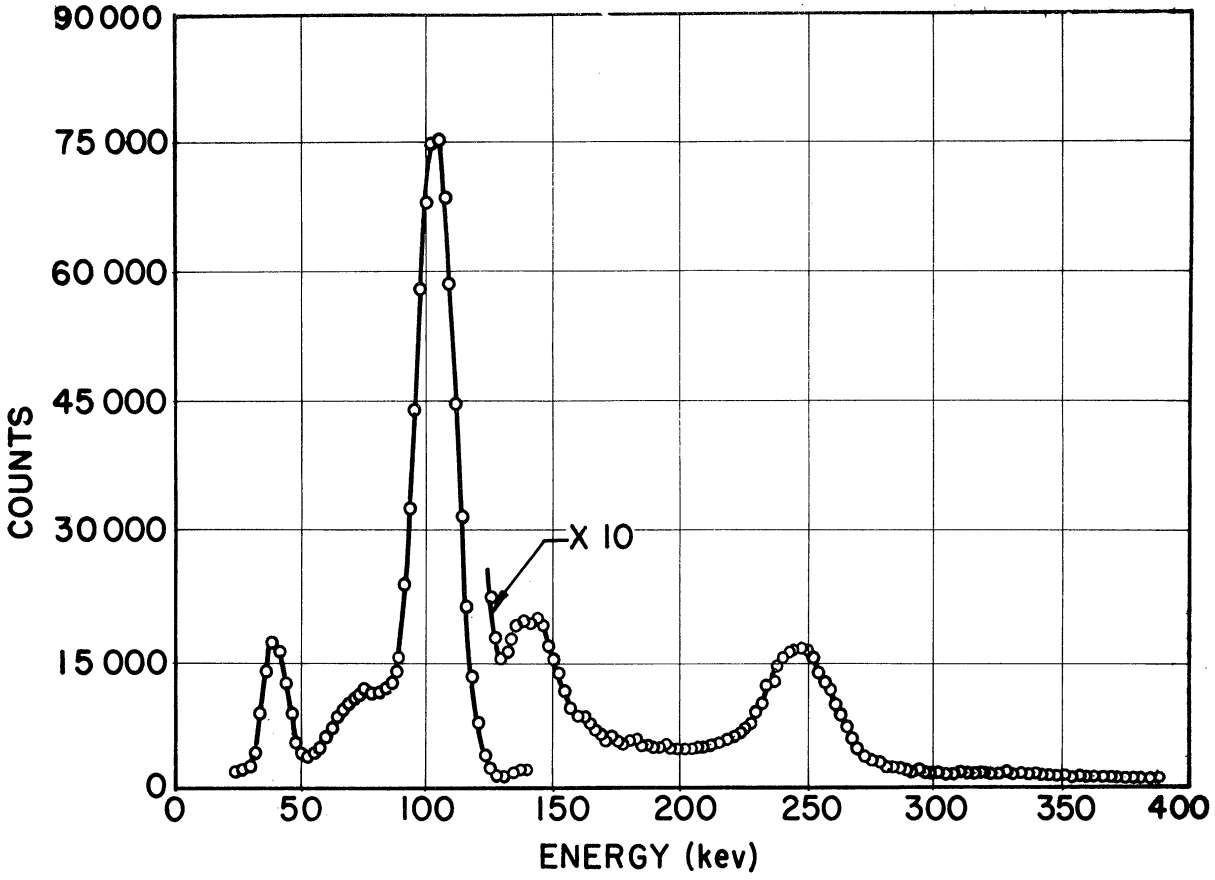

Figure 21. Scintillation Spectrum of Gamma Rays in Eu^{155}.

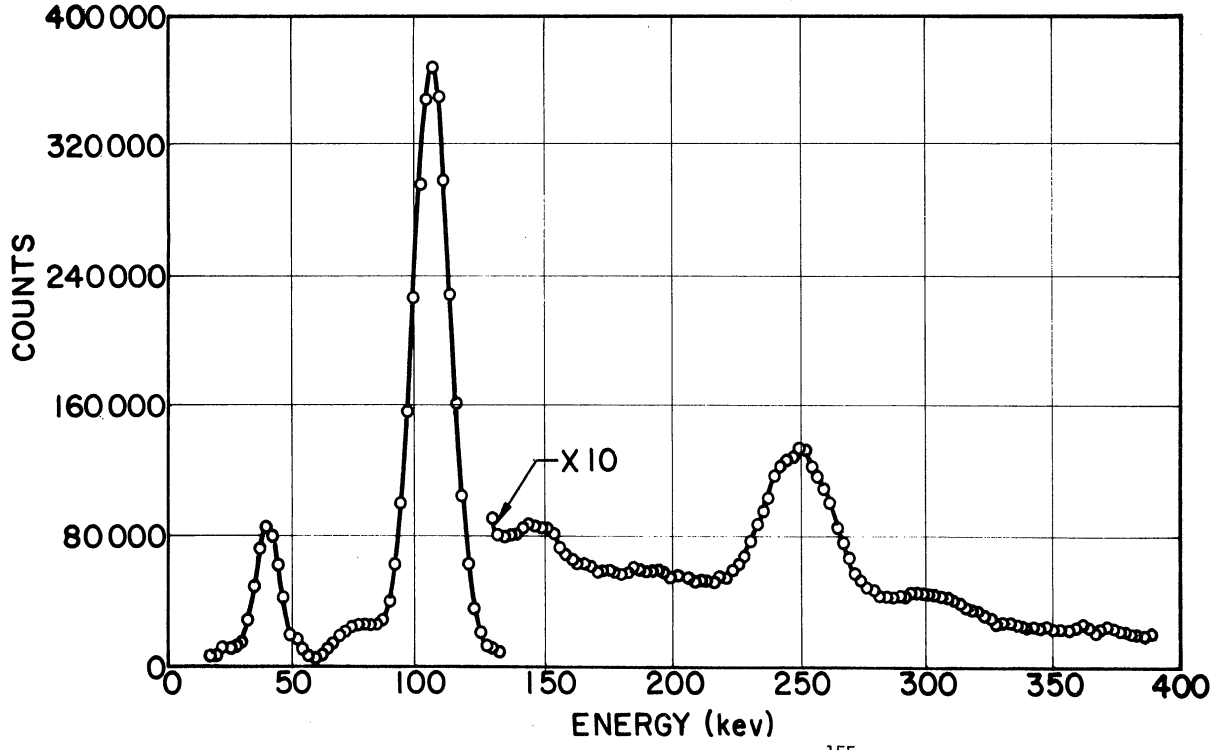

Figure 22. Spectrum of Gamma Rays in Eu^{155} taken with Source in a 2-in. Well Crystal.

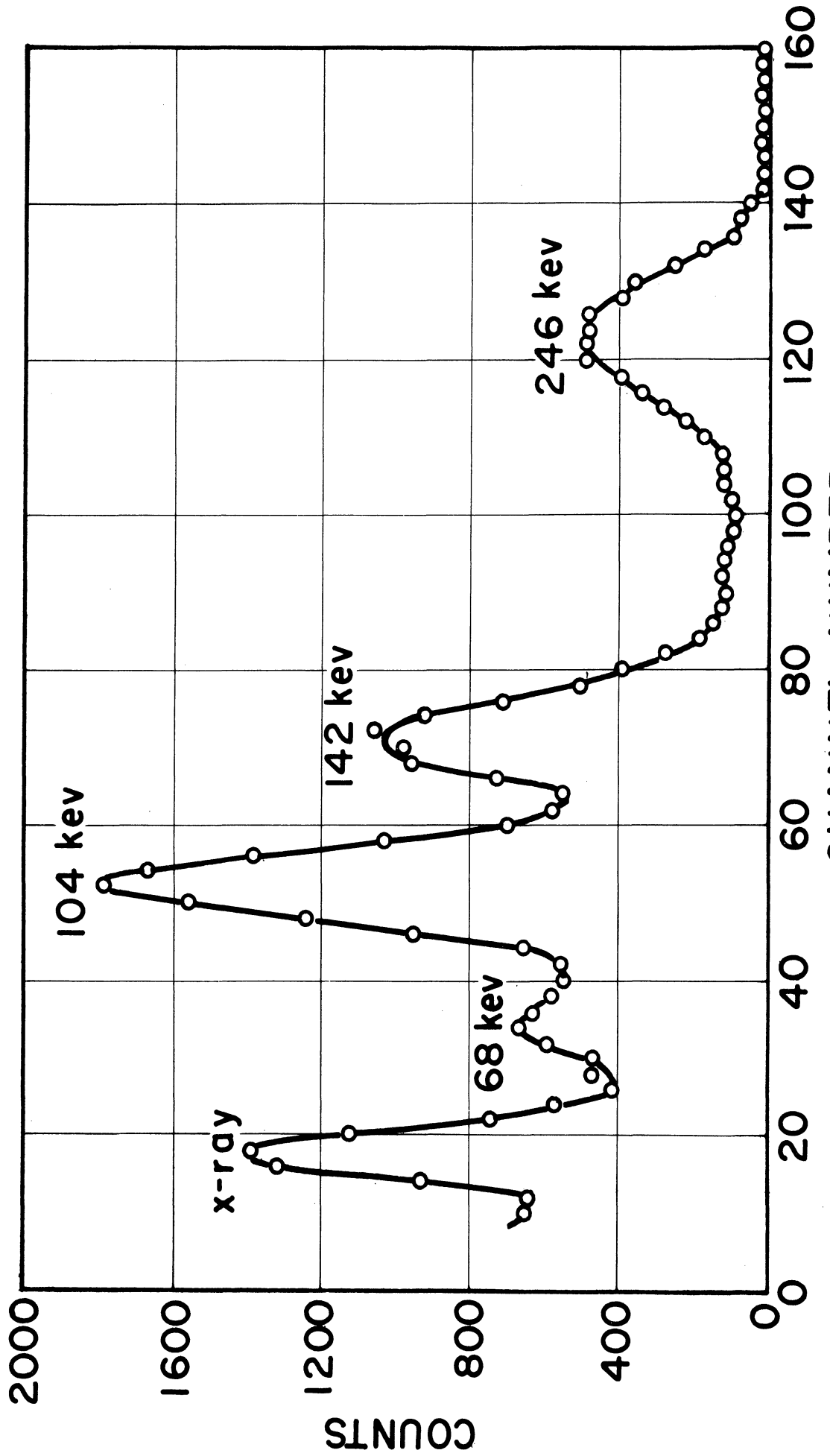

Figure 23. Spectrum of $_{15}$Gamma Rays in Coincidence with the X-Ray in Decay of Sm^{153}.

The spectrum of coincidences with the 142-kev gamma ray, Figure 24, indicates that the x-ray and 104-kev transitions are in coincidence with the 142-kev transition. Similarly, Figure 25 indicates that the x-ray and 142-kev transitions are the prominent coincidences with the 104-kev gamma ray. A weak coincidence with the 68-kev gamma ray is possible in both the 104-kev and 142-kev coincidence spectra.

Figure 26A is the spectrum of gamma rays coincident with the 246-kev photopeak. Coincidences are indicated with the x-ray and with weak gamma rays of about 68 kev and 103 kev. Because of the strong peak at the x-ray energy, selective absorption was used to determine whether part of this peak is due to a gamma ray with an energy close to that of the x-ray. The coincidence measurements with the 246-kev gamma ray were repeated, using on successive runs (0.076 ± 0.008) gm/cm^2 of Ce, (0.060 ± 0.005) gm/cm^2 of Pr, and no absorber (except a β shield) in front of the crystal feeding the multi-channel analyzer. The coincidence spectrum with the Ce absorber is shown in Figure 26B and indicates considerable attenuation of the x-ray, whereas the coincidence spectrum with the Pr absorber shows much less attenuation, as shown in Figure 26C. There results can be adequately explained by assuming that the entire photopeak is due to the x-ray.

In all cases the accidental spectra were small and were subtracted to get the curves shown. All of the gamma rays decayed with the proper half-life.

The proposed decay scheme is shown in Figure 27. It agrees with the decay scheme reported by Schmid and Burson[86] except for the

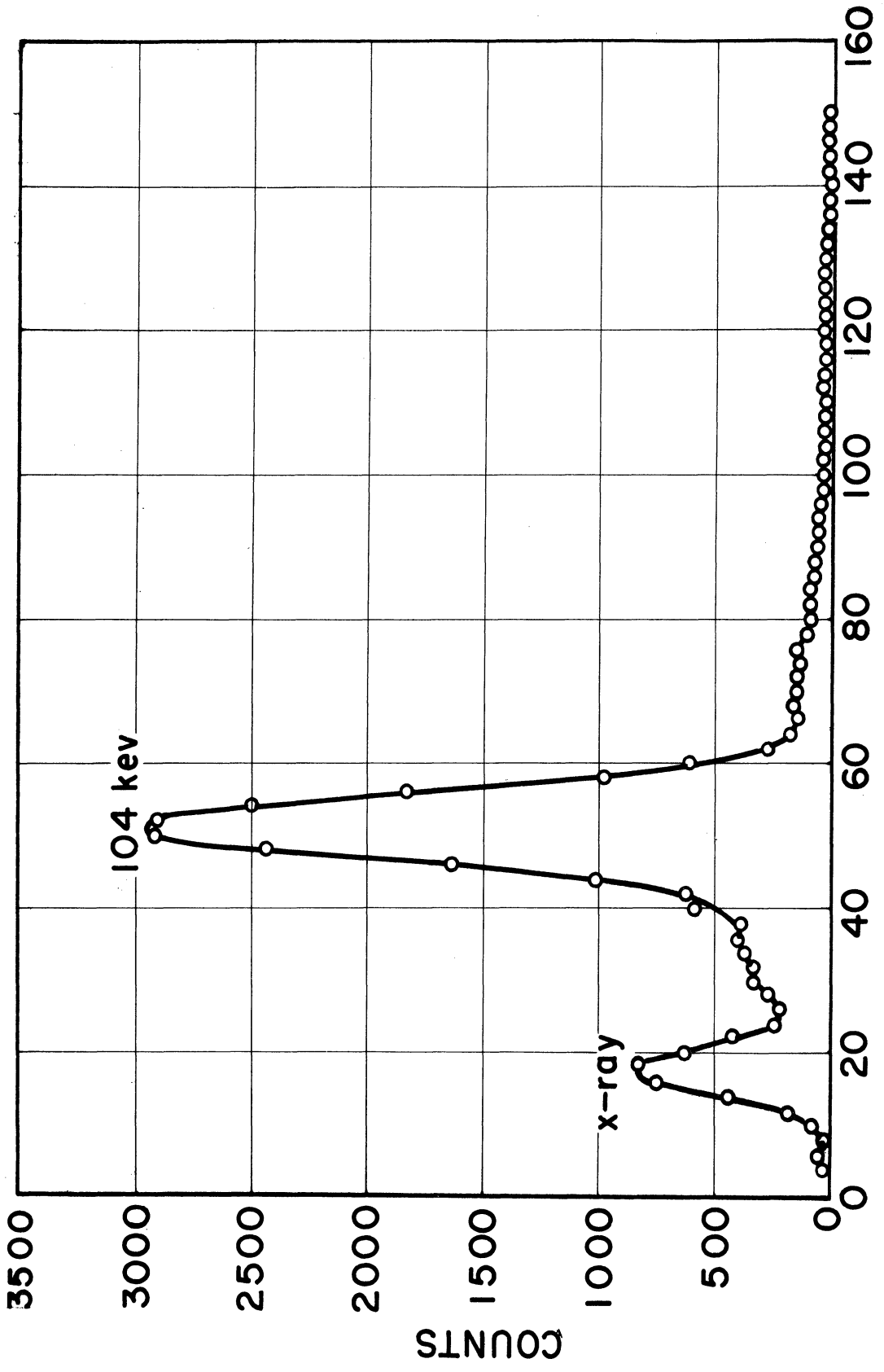

Figure 24. Spectrum of Gamma Rays in Coincidence with the 142-kev Gamma Ray in Decay of Sm^{155}.

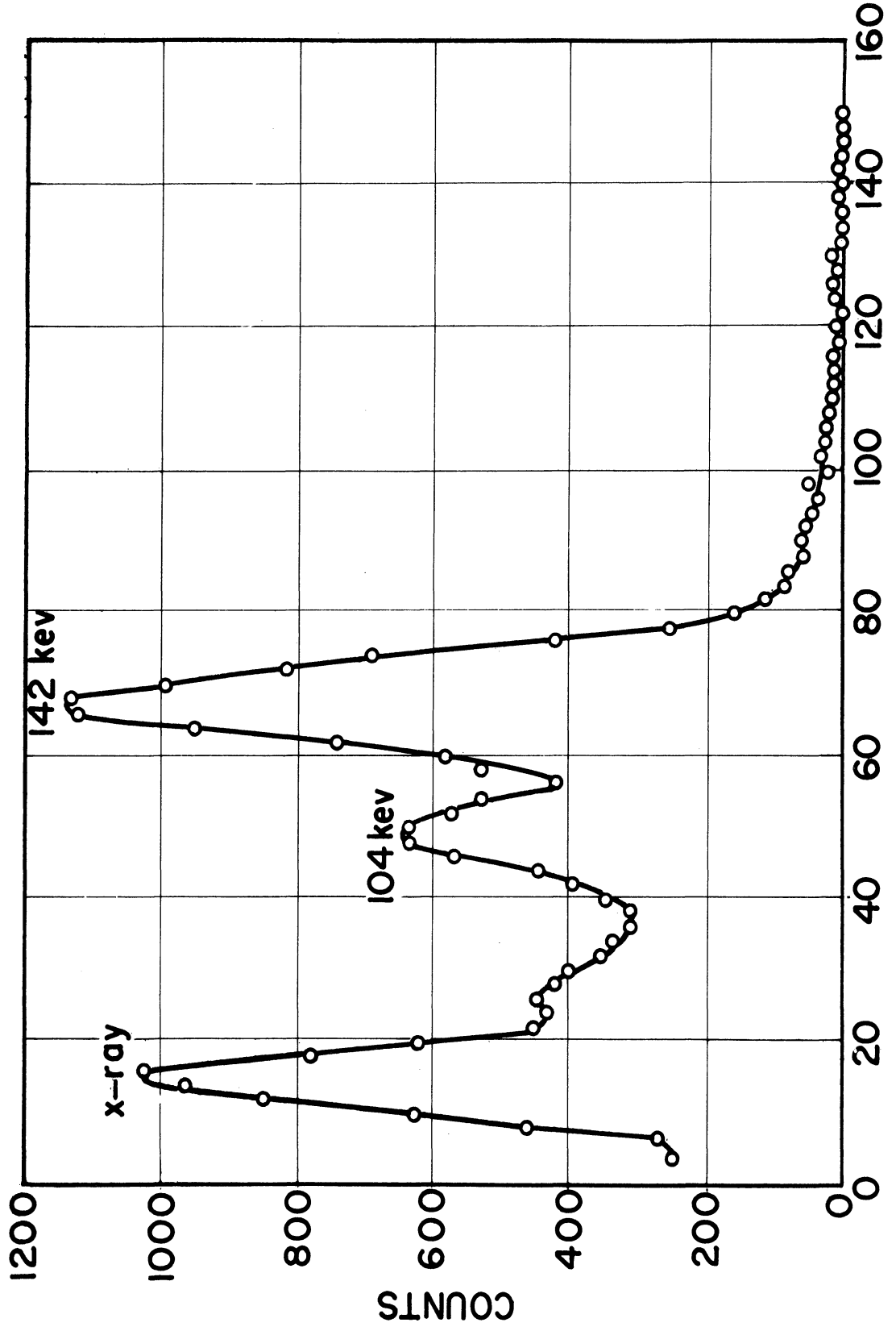

Figure 25. Spectrum of Gamma Rays in Coincidence with the 104-kev Gamma Ray in Decay of Sm^{155}.

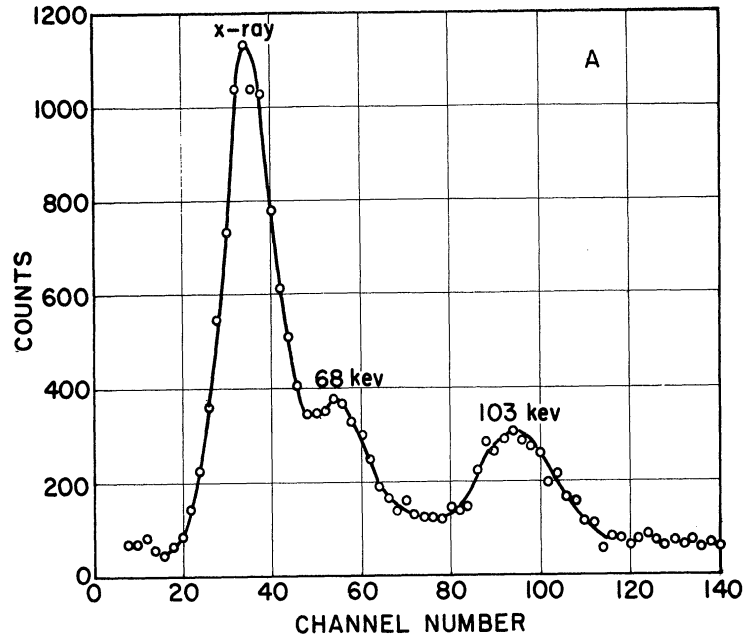

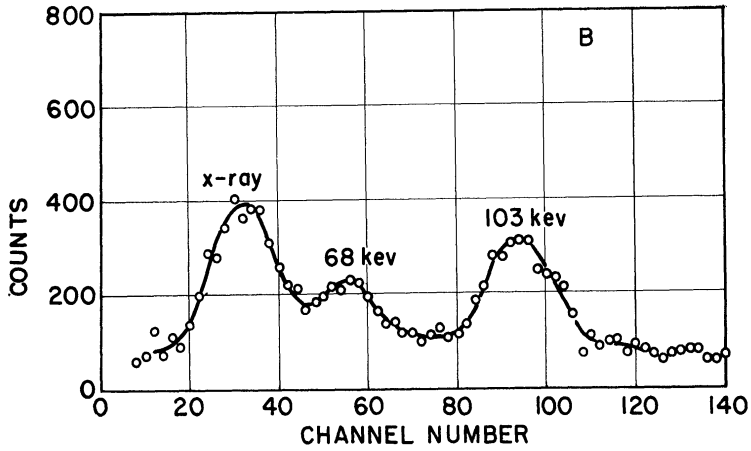

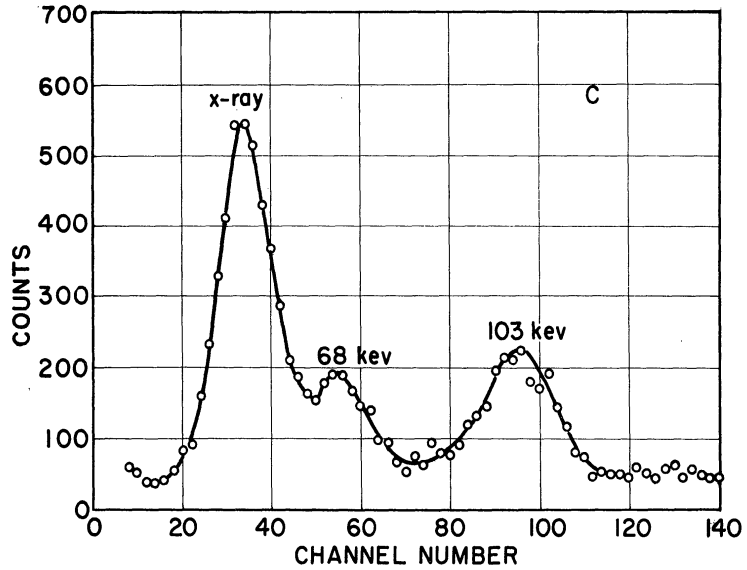

Figure 26. Spectra of gamma rays in coincidence with the 246-kev gamma ray in decay of Sm^{155}, using various absorbers in front of the crystal feeding the multi-channel analyzer. Curve A was taken with a β absorber. Curve B was taken with an additional (0.076 ± 0.008) gm/cm^2 Ce absorber. Curve C was taken with an additional (0.060 ± 0.005) gm/cm^2 Pr absorber.

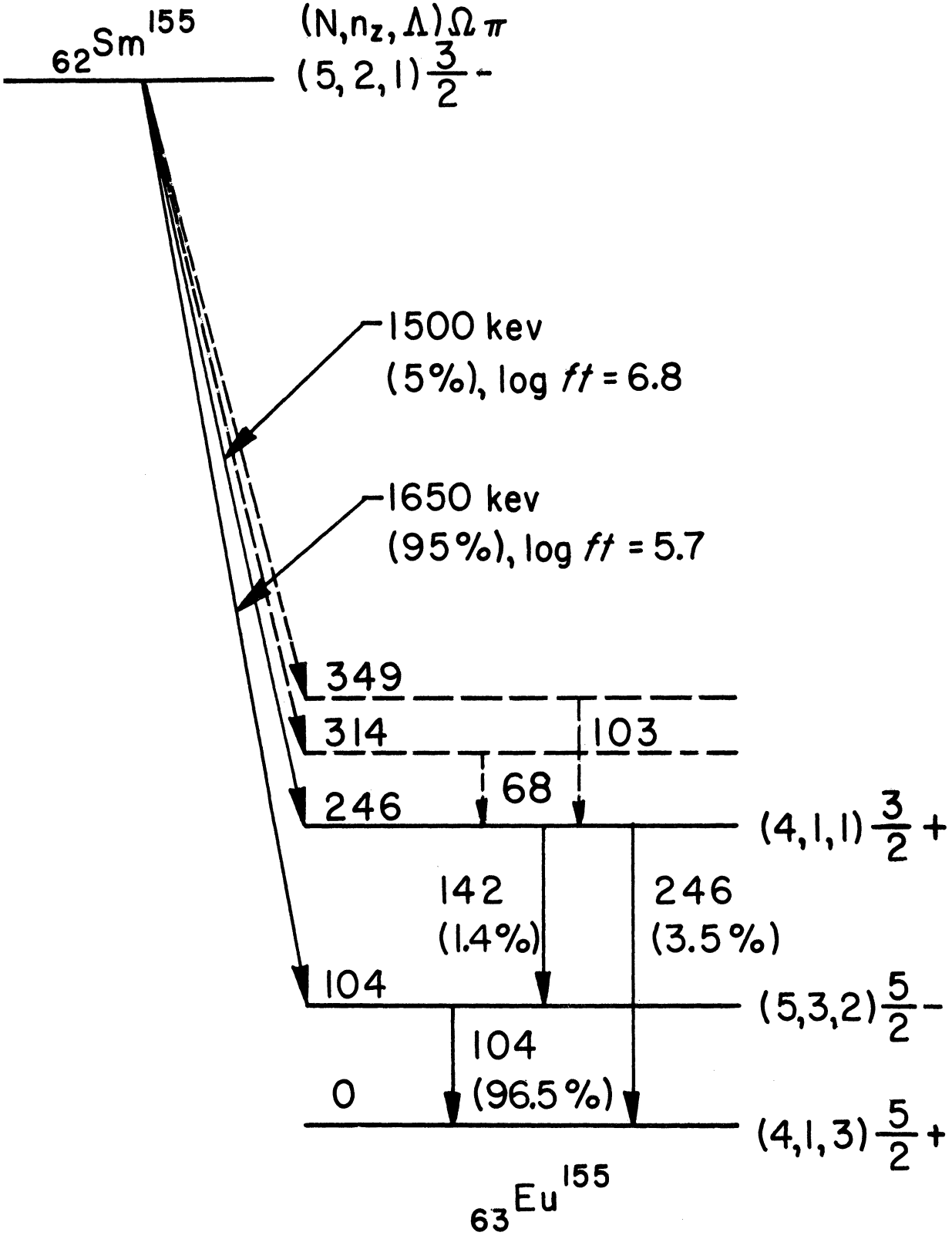

Figure 27. Decay Scheme of Sm^{155}.

weakly fed levels at 314 kev and 349 kev, and the corresponding gamma transitions. The additional levels are supported by the coincidence measurements and by the sum peak observed between the x-ray and the 246-kev transition. Schmid and Burson[86] explained the lack of a beta transition to the ground state of Sm^{155} in terms of the selection rules for deformed nuclei proposed by Alaga.

The intensities have been calculated from the gamma spectrum, correcting for absorbers, crystal efficiency, and the internal conversion coefficients[86] of 0.27 for the 104-kev transition and 0.16 for the 142-kev transition. In the calculation, the internal conversion coefficient for the 246-kev transition was assumed to have the theoretical value[50] for a M1 transition on the basis of a K/L ratio equal to eight.[85]

On the basis of relative source strengths and counting rates in the coincidence measurements, the intensity of the 103-kev transition is on the order of magnitude of 2% of the intensity of the 142-kev gamma ray, with the 68-kev transition being somewhat weaker. The very weak intensity of the 103-kev — 246-kev cascade in comparison with the 104-kev — 142-kev cascade explains the low number of counts at 246 kev in the 104-kev coincidence spectrum.

A number of weak lines observed in the internal conversion measurements are not shown in the decay scheme. These gamma rays are too weak to be observed in the gamma ray spectra or in the coincidence measurements. On the basis of the coincidence measurements the intensity of any of these transitions is less than about 0.1% of the total number of disintegrations. However, the uncertainty in the position of these transitions in the decay scheme may allow somewhat higher intensities.

Directional Correlation Measurements on 142-kev — 104-kev Cascade

The directional correlation was measured by accepting a range of energies from 95 kev to 150 kev in both pulse-height analyzers. The interference between the gamma rays in this energy range and the Comptons of higher-energy gamma rays was found to be 10.5 ± 1.1%. After subtracting this interference and correcting for finite resolution,[47] the expansion coefficients were found to be $A_2 = -0.086 \pm 0.028$ and $A_4 = -0.057 \pm 0.050$. Interference from the 103-kev — 142-kev cascade and the 103-kev — 104-kev cascade is not significant due to the low intensity of the 103-kev transition.

For a nuclear deformation of .33 for $_{63}Eu^{155}$, the Nilsson model[16] predicts a ground-state spin of 5/2+. The measured spin[79,80] of 5/2+ for Eu^{153} supports this. The spin[79,80] of 5/2- for Eu^{151} is due to the small deformation and the corresponding change in the position of the energy levels. For $_{62}Sm^{155}$, the Nilsson calculations[16] predict a spin of 3/2- or 5/2+ for the ground state. A spin[88,89] of 3/2- for the ground state of $_{64}Gd^{157}$ and the lack of a beta transition between the ground states of Sm^{155} and Eu^{155} support a spin of 3/2- for the ground state of Sm^{155}.

The calculated log ft values are 5.7 for the 1.65-Mev beta ray and 6.8 for the 1.50-Mev beta transition. The internal conversion coefficients[86] of 0.27 ± 0.06 for the 104-kev transition and 0.16 ± 0.06 for the 142-kev gamma ray indicate that both transitions are predominately E1. These data indicate that the spin of the 246-kev level is 1/2+, 3/2+, or 5/2+, and that the spin of the 104-kev level is 5/2- or 3/2-. The possible spin assignments for the 246-kev level and the K/L ratio[85] of about 8 for the 246-kev gamma ray agree in indicating that the 246-kev transition is M1. If the experimental internal conversion coefficients

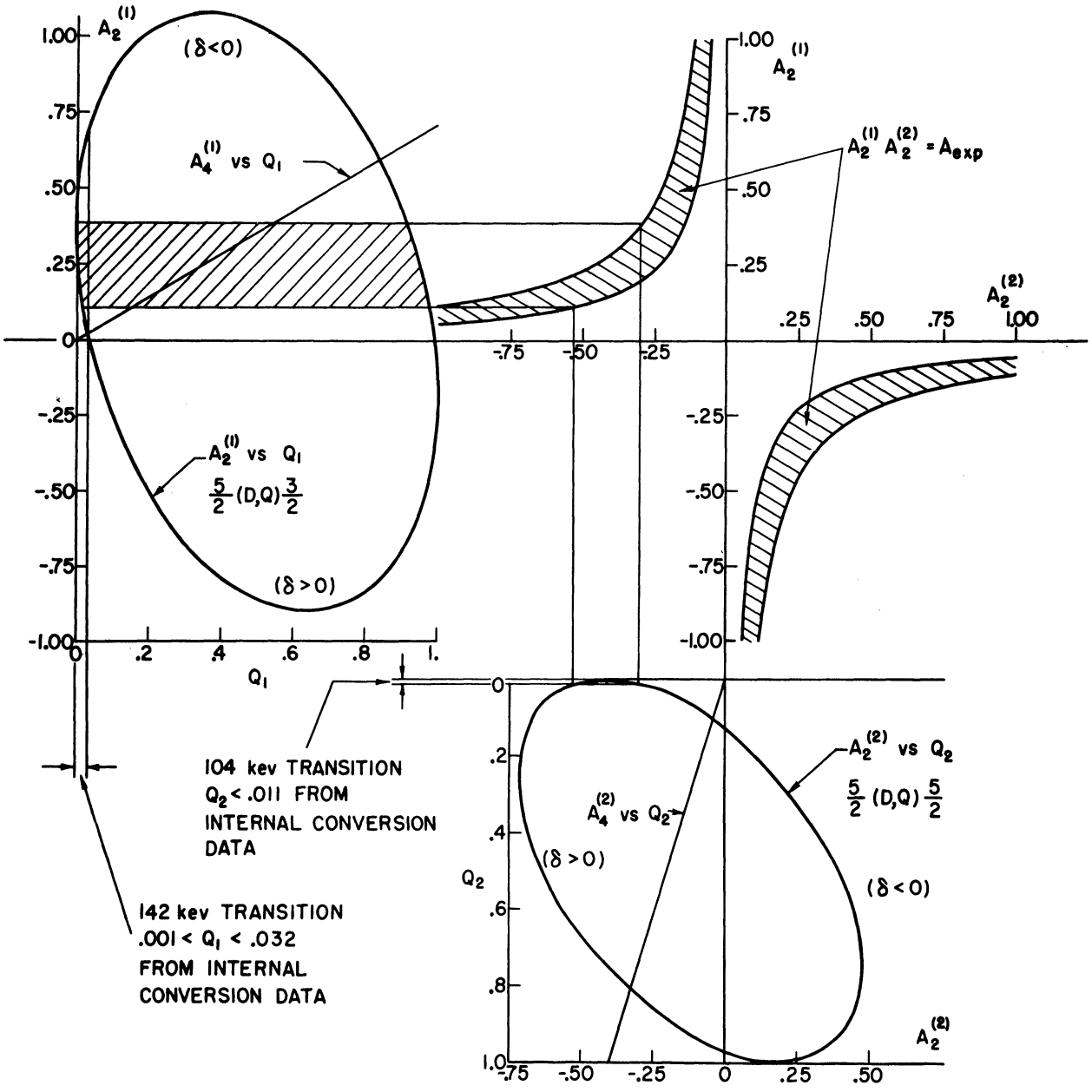

Figure 28. Analysis of the 142-kev — 104-kev directional correlation in Eu^{155} in terms of a 3/2(D,Q)5/2(D,Q)5/2 sequence.

are interpreted with the K conversion coefficients calculated by Sliv,[50] the 104-kev transition is found to be an E1 + M2 mixture with $0.001 \leq Q \leq 0.032$. The graphical analysis[33] of the directional correlation data in terms of a 3/2(D,Q)5/2(D,Q)5/2 sequence is shown in Figure 28. The limits of quadrupole content consistent with the internal conversion data are indicated. A 3/2(D,Q)3/2(D,Q)5/2 sequence is also allowed by the angular correlation and conversion data. For a deformation of 0.33 and a ground-state spin of 5/2 + for Eu^{155}, the Nilsson model[16] predicts low-lying excited states of 3/2+ and 5/2-. Therefore the 3/2(D,Q)5/2(D,Q)5/2 cascade is favored. Other spins for the ground states of Sm^{155} and Eu^{155} would permit different interpretations of the directional correlation data.

CHAPTER VII

FUTURE DEVELOPMENTS

The two level structures investigated in the present study form a small part of the total research being conducted in low-energy nuclear physics. However, much experimental information remains to be gathered in order to establish a better knowledge of nuclear properties. With the improvement in experimental techniques, many measurements can be made which were previously impossible. Thus, the 256-channel analyzer in conjunction with the fast-slow coincidence apparatus and the gate circuit has made possible the observation of very weak gamma rays, such as the 422-kev gamma ray in Eu^{153}. This gamma ray has an intensity of about 10^{-4} of the 103-kev transition intensity, and the 422-kev — 173-kev cascade intensity is about 10^{-6} of that for the 103-kev transition.

The development of automatic data recording on directional correlation apparatus makes feasible the analysis of many weak cascades which have not been done previously because of the time required.

An important tool recently acquired in the laboratory is a Van de Graaf generator. This will make possible the study of isotopes made by the (n,2n) reaction. The study of higher excited energy levels through neutron-capture gamma rays can also be done with such an instrument.

Among the possible improvements in experimental apparatus in the future is the development of improved gamma ray detectors. Solid state ionization counters with good resolution for charged particles have

been developed. If a suitable high-Z material can be found for such a gamma ray detector, the improvement in resolution would greatly stimulate experimental developments. Many more gamma rays could be resolved, and previously impossible directional correlation measurements could be done.

Before the systematics of odd-A nuclei will be well-established, much experimental research needs to be done, particularily in the intermediate regions which exist between nuclei near closed shells and strongly deformed nuclei. The method recently developed in analyzing double mixture cascades in directional correlations will aid in studying these nuclei.[13,33] Although the main transitions in many even-even nuclei have been studied, present equipment allows further investigation of weak transitions. In addition to studying the energies, spins, and parities of excited levels, the further determination of transition probabilities between the levels would be valuable. Continued development in our knowledge of the systematics of nuclear properties will allow the theorist to further check the validity of nuclear models.

The predictions made by nuclear models in most cases are limited and also frequently fail to treat the intermediate regions. Theories must be developed which predict more properties of nuclear levels and which have a wider range of applicability. The work of Davydov and Filippov[11,12] on the level structure of nuclei which do not have axial symmetry has proved valuable in this respect. Their study has been mainly restricted to even-even nuclei, and they are now extending it to odd-A nuclei. Their results are expected to throw more light on the properties of levels in such deformed nuclei.

It is felt that continued experimental research will greatly help in establishing a more complete picture of nuclear properties. With the constant efforts of the experimentalist and the theorist, our understanding of the nucleus will continue to improve.

BIBLIOGRAPHY

1. Mayer, M. G. Phys. Rev. 75, 1969 (1949).

2. Haxel, Jensen, and Suess, Phys. Rev. 75, 1766 (1949).

3. Mayer, M. G. and Jensen, J. H. Elementary Theory of Nuclear Shell Model. New York: John Wiley and Sons, Inc., 1955.

4. Jensen, J. H. in Beta and Gamma Ray Spectroscopy, ed. by K. Siegbahn, Amsterdam: North-Holland Publishing Co., 1955.

5. Bethe, H. A. and Morrison, P. Elementary Nuclear Theory. New York: John Wiley and Sons, Inc., 1956.

6. Bohr, A. Dan. Vid. Selsk., Mat. Fys. Medd. 26, No. 14 (1952).

7. Bohr, A. and Mottelson, B. R. Dan. Vid. Selsk. Mat. Fys. Medd. 27, No. 16 (1953).

8. Alaga, Alder, Bohr, and Mottelson, Dan. Vid. Selsk. Mat. Fys. Medd. 29 No. 9, 1955.

9. Alder, Bohr, Huus, Mottelson, and Winther, Revs. Mod. Phys. 28 432 (1956).

10. G. Scharff-Goldhaber and J. Weneser, Phys. Rev. 98, 212 (1955).

11. Davydov, A. S. and Filippov, G. F. Nuclear Phys. 8, 237 (1958).

12. Davydov, A. S. and Filippov, G. F. JETP 36, 1497 (1959).

13. Arns, R. G. Doctoral Thesis, University of Michigan, 1959.

14. Nilsson, S. G., Dan. Vid. Selsk. Mat Fys. Medd. 29, No. 16 (1955).

15. Mottelson, B. R. and Nilsson, S. G. Dan. Vid. Selsk. Mat. Fys. Skrifter 1, No. 8, 1959.

16. Mottelson, B. R. and Nilsson, S. G. Phys. Rev. 99, 1615 (1955).

17. Alaga, G. Phys. Rev. 100, 432 (1955).

18. Alaga, G. Nuclear Phys. 4, 625 (1957).

19. Hamilton, D. R. Phys Rev. 58, 122 (1940).

20. Brady, E. L. and Deutsch, M. Phys. Rev. 72, 870 (1947).

21. Brady, E. L. and Deutsch, M. Phys. Rev. 74, 1541 (1948).

22. Goertzel, G. Phys. Rev. 70, 897 (1946).

23. Falkoff, D. L. Doctoral Thesis, University of Michigan, 1948.

24. Falkoff, D. L. and Uhlenbeck, G. E. Phys. Rev. 79, 323 (1950).

25. Ling, D. S. and Falkoff, D. L. Phys. Rev. 76, 1639 (1949).

26. Racah, G. Phys. Rev. 84, 910 (1951).

27. Lloyd, S. P. Phys. Rev. 85, 904 (1952).

28. Coester, F. and Jauch, J. Helv. Phys. Acta 26, 3 (1953).

29. Frauenfelder, H. in Beta and Gamma Ray Spectroscopy, ed. by K. Siegbahn, Amsterdam: North-Holland Publishing Co., 1955.

30. Heitler, W. Quantum Theory of Radiation. New York: Oxford University Press, 1944.

31. Yang, C. N. Phys. Rev. 74, 764 (1948).

32. Ferentz, M. and Rosenzweig, N. Argonne Natl. Lab. Report 5324, 1955.

33. Arns, R. G. and Wiedenbeck, M. L. Phys. Rev. 111, 1631 (1958).

34. Arns, R. G. and Wiedenbeck, M. L. University of Michigan Res. Inst. Report 2375-3-T, January, 1958.

35. Stewart, M. G. Doctoral Thesis, The University of Michigan, 1955.

36. Scharenberg, R. Doctoral Thesis, The University of Michigan, 1955.

37. Arns, R. G. Private communication.

38. Garwin, R. L. Rev. Sci. Inst. 21, 569 (1950).

39. Garwin, R. L. Rev. Sci. Inst. 24, 618 (1953).

40. Johnstone, C. W. Nucleonics, 11, 36 (1953).

41. Lu, D. C. Doctoral Thesis, The University of Michigan, 1954.

42. De Benedetti, S. and Findley, R. W. Handbuch der Physik, ed. by S. Flügge. Berlin: Springer-Verlag, (1958), Vol. 45, p. 233.

43. Rose, M. E. Phys. Rev. 91, 610 (1953).

44. Lawson, J. S., Jr. and Frauenfelder, H. Phys. Rev. 91, 649 (1953).

45. Church, E. L. and Kraushaar, J. Phys. Rev. 88, 419 (1952).

46. Feingold, A. M. and Frankel, S. Phys. Rev. 97, 1025 (1955).

47. Arns, Sund, and Wiedenbeck, The University of Michigan Res. Inst. Report 2375-4-T, February, 1959.

48. Millman, J. and Taub, H. Pulse and Digital Circuits. New York: McGraw-Hill Book Company, Inc. (1956), 445-447.

49. Rose, M. E. in Beta and Gamma Ray Spectroscopy ed. by K. Siegbahn. Amsterdam: North-Holland Publishing Co., (1955), Appendix IV.

50. Sliv, L. A. and Band, I. M. Leningrad Physico-Technical Institute Report, 1956 (Translation: Report 57 ICC KL, issued by Physics Dept. University of Illinois, Urbana, Illinois (unpublished)).

51. McCutchen, C. W. Nuclear Phys. 5, 187 (1958).

52. Mihelich, J. W. Phys. Rev. 87, 646 (1952).

53. Siegbahn, K. Arkiv Fysik 4, 223 (1952).

54. Graham, R. L. and Walker, J. Phys. Rev. 94, 794A (1954).

55. Lee, M. R. and Katz, R. Phys. Rev. 93, 155 (1954).

56. McGowan, F. K. Phys. Rev. 93, 163 (1954).

57. Marty, M. Compt. rend. 238, 2516 (1954).

58. Marty, M. J. Phys. Radium 16, 458 (1955).

59. Anderson, B. Proc. Phys. Soc. (London) 69A, 415 (1956).

60. Dubey, Mandeville, and Rothman, Phys. Rev. 103, 1430 (1956).

61. Joshi, Subba Rao, and Thosar, Proc. Indian Acad. Sci. 45A, 390 (1957).

62. Beckman, O. Nuclear Inst. 3, 27 (1958)

63. Cork, Brice, Helmer, and Woods, Phys. Rev. 110, 526 (1958).

64. Klove, A. and Storruste, A. Archiv Math. Naturvidenskab 54, 57 (1958).

65. Walters, Rasmussen, and Mark, Nuclear Phys. 15, 653 (1960).

66. Church, E. L. and Goldhaber, M. Phys. Rev. 95, 626A (1954).

67. Cohen, Burde, and Ofer, Bull. Research Council Isreal 5A, 87A (1955).

68. Bhattacherjee, S. K. and Raman, S. Nuclear Phys. 1, 486 (1956).

69. Bisi, Germagnoli, and Zappa, Nuclear Phys. 1, 593 (1956).

70. Gupta, R. K. and Jha, S. Nuova cimento 4, 88 (1956).

71. Marty, N. and Vergnes, M. Compt. rend. 242, 1438 (1956).

72. Joshi, M. C. and Subba Rao, B. N., Proc. Indian Acad. Sci. 46, 430 (1957).

73. Antoneva, Bashilov, Dzhelepov, and Preobrazhenskii, Izvest, Akad. Nauk S.S.S.R., Ser. Fiz. 22, 135 (1958).

74. Vergnes, M. Ann. phys. 5, 11 (1960).

75. Graham, Ewan, and Geiger, Bull. Am. Phys. Soc. Ser. II 5, 21 (1960).

76. Class, C. M. and U. Meyer-Berkout, Nuclear Phys. 3, 656 (1957).

77. Johnson, W. H., Jr. and Nier, A. O. Phys. Rev. 105, 1014 (1957).

78. de Boer, Martin, and Marmier, Helv. Phys. Acta 31, 578 (1958).

79. Mack, J. E. Revs. Modern Phys. 22, 64 (1950).

80. Bleaney, B. and Low, W. Proc. Phys. Soc. (London) 68A, 55 (1955).

81. Cabezas, Lipworth, Marrus, and Winocur, Phys. Rev. 118, 233 (1960).

82. Pool, M. L. and Quill, L. L. Phys. Rev. 53, 437 (1938).

83. Inghram, Hayden, and Hess, Phys. Rev. 71, 643 (1947).

84. Winsberg, L. NNES 9, Div. IV, paper 196 (1951).

85. Rutledge, Cork, and Burson, Phys. Rev. 86, 775 (1952).

86. Schmid, L. C. and Burson, S. B. Phys. Rev. 115, 447 (1959).

87. Bell, P. R. in Beta and Gamma Ray Spectroscopy ed. by K. Siegbahn. Amsterdam: North-Holland Publishing Co., (1955) p. 155.

88. Low. W. Phys. Rev. 103, 1309 (1956).

89. Speck, D. R. Phys. Rev. 101, 1725 (1956).